





## Thalweg and Ridge Network Extraction From Unaltered Topographic Data as a Basis for Terrain Partitioning

 Giovanni Moretti<sup>1</sup>  and Stefano Orlandini<sup>1</sup> 
<sup>1</sup>Dipartimento di Ingegneria Enzo Ferrari, Università degli Studi di Modena e Reggio Emilia, Modena, Italy

### Key Points:

- Physically meaningful thalweg and ridge networks can be extracted automatically from any high-resolution grid digital elevation model
- Depressions and nested systems of exorheic and endorheic basins are handled without the need to alter the observed topographic data
- Thalweg and ridge networks can be obtained at the desired level of detail and are presented here as novel bases for terrain partitioning

### Supporting Information:

Supporting Information may be found in the online version of this article.

### Correspondence to:

 S. Orlandini,  
[stefano.orlandini@unimore.it](mailto:stefano.orlandini@unimore.it)

### Citation:

 Moretti, G., & Orlandini, S. (2023). Thalweg and ridge network extraction from unaltered topographic data as a basis for terrain partitioning. *Journal of Geophysical Research: Earth Surface*, 128, e2022JF006943. <https://doi.org/10.1029/2022JF006943>

Received 28 SEP 2022

Accepted 3 APR 2023

### Author Contributions:

**Conceptualization:** Giovanni Moretti, Stefano Orlandini

**Formal analysis:** Giovanni Moretti, Stefano Orlandini

**Investigation:** Giovanni Moretti, Stefano Orlandini

**Methodology:** Giovanni Moretti, Stefano Orlandini

**Software:** Giovanni Moretti

**Validation:** Giovanni Moretti, Stefano Orlandini

**Writing – original draft:** Giovanni Moretti, Stefano Orlandini

© 2023. The Authors.

 This is an open access article under the terms of the [Creative Commons Attribution License](https://creativecommons.org/licenses/by/4.0/), which permits use, distribution and reproduction in any medium, provided the original work is properly cited.

**Abstract** High-resolution grid digital elevation models (DEMs) are increasingly used by scientists and engineers to describe the current state and evolution of Earth and planetary topography. These data, however, are commonly altered by depression filling and grid coarsening procedures. Alteration of observed topographic data may cause significant information loss and limit the capabilities of models. This study shows that physically meaningful thalweg and ridge networks can be extracted automatically from any unaltered high-resolution grid DEM, and that these networks can be used as bases for terrain partitioning. The slopeline network connecting grid cell centers is used to identify ridge points as those grid cell border midpoints and vertices that are not crossed by slopelines. From each ridge point, the average length of the two slopelines extending on the opposite slopes of the ridge until they rejoin is then computed. Based on these lengths, exorheic and endorheic basins are identified. Thalwegs of exorheic and endorheic basins are finally connected through spilling saddles to form the thalweg network. The related ridge network is identified based on neighboring relationships between ridge points. Thalweg and ridge networks are hierarchized using the well-known concept of drainage area and an extended concept of dispersal area to inform terrain partitioning at any level of detail. Observed topographic features are well reproduced by extracted networks. The impact of preserving depressions over mountain areas is evaluated, and the benefits from unstructured terrain partitioning based on thalweg and ridge networks in the description of flood plain inundation are illustrated.

**Plain Language Summary** Detailed topographic data are increasingly used by scientists and engineers to describe the current state and evolution of Earth and planetary topography. In current models, however, depressions are commonly filled for model simplicity, and grids are normally coarsened for computational efficiency. Alteration of observed topographic data may cause a significant information loss and limit the capabilities of models. In this study, it is shown that the lines following the lowest part of a valley or channel (thalwegs) and the lines of intersection at the top between opposite slopes (ridges) are the essential topographic features (bases) that need to be extracted from observed topographic data and retained when terrain is partitioned. New terrain analysis methods are developed to extract thalweg networks connecting depression (endorheic) and drainage (exorheic) basins, and to identify physically meaningful ridge networks. Observed topographic features are well reproduced by extracted networks. The impact of preserving depressions over mountain areas is evaluated, and the benefits from unstructured terrain partitioning based on thalweg and ridge networks in the description of flood plain inundation are illustrated. The developed methods provide a new pathway for scientists and engineers to rigorously incorporate detailed topographic data into their descriptions of Earth surface processes.

## 1. Introduction

Increasingly detailed observations of rocky and icy bodies in our solar system reveal dramatic diversity in surface topographic features (Black et al., 2017; Head et al., 2003). Earth topography helps scientists determine how rivers and streams drain through the landscape, where lowlands are prone to flooding, how plate tectonics or erosion are building or wearing away mountains, where hills may be prone to landslides, or how a volcanic eruption changed the shape of a mountain (Passalacqua et al., 2015; Robinson et al., 2017). Topography is also one of the factors that influences the existence of particular ecosystems (Frolking et al., 2009; Shugart et al., 2010). Therefore, topography is one of the factors that scientists can use to predict where certain plants or animals, such as endangered species, might be found. Planetary topography has been largely investigated in the last two decades (Perron et al., 2007; Smith et al., 1999). Black et al. (2017) compared topography at a range of scales with mapped river drainages to provide new insights into the topography-generating mechanisms on Earth, Mars, and Titan. As reported by Burr (2017), quantifying discrepancies between drainage networks and surrounding

Writing – review & editing: Giovanni Moretti, Stefano Orlandini

topography provides a new understanding of the mechanisms by which this topography is generated. Grid digital elevation models (DEMs) having a resolution of 1 m or less are increasingly used by scientists and engineers to describe the current state and evolution of Earth and planetary topography (Tarolli, 2014). In existing models for the description of Earth surface processes, however, depressions observed in high-resolution topographic data are commonly filled for model simplicity, and grids are normally coarsened for computational efficiency. Depression filling (DF) is applied before and/or after grid coarsening (Moretti & Orlandini, 2018). In all cases, the alteration of observed topographic data may cause significant information loss and limit the capabilities of models (Lindsay & Creed, 2005; Moretti & Orlandini, 2018).

Depression filling is commonly applied in drainage basin hydrology as a means to a fully integrated flow path network (Callaghan & Wickert, 2019; O'Callaghan & Mark, 1984). With DF, all grid cells in a drainage basin, with the exception of the outlet cell, are processed to eliminate depressions by simulated filling; a drainage direction is subsequently imposed on the flat area that results from the filling procedure (Barnes et al., 2014, 2020, 2021; Grimaldi et al., 2007; Hutchinson, 1989; Martz & Garbrecht, 1992, 1999). As an alternative to raising cell elevations to remove depressions, Martz and Garbrecht (1999) proposed a method that incorporates constrained breaching of the depression outlets. Barnes et al. (2014) implemented the priority flood algorithm that optimizes the DF procedure to minimize the raising of cells. To minimize the impact of DF, Barnes et al. (2020, 2021) developed a depression hierarchy data structure and they routed water in a similar way as standard flow accumulation algorithms until runoff filled depressions, which then overflowed and spilled into their neighbors. Depression filling has been considered as a measure of correction from different sources of errors causing grid cell scale artificial depressions in topographic data (Lindsay & Creed, 2005). It is however difficult, if not impossible, to determine whether a grid cell scale depression is natural or artificial. In addition, with DF not only grid cell scale depressions are removed but also large depression (endorheic) basins and drainage (exorheic) basins flowing into canyons that are lost when high-resolution topographic data are coarsened (Moretti & Orlandini, 2018). Depression filling has been largely accepted in drainage basin hydrology and remains a possible modeling option when depressions play a minor role in the investigated Earth surface processes (David et al., 2023). In general, however, it is scientifically unsound to alter observed topographic data by filling depressions without first evaluating their role in Earth surface processes. In fact, DF makes it impossible to investigate the role of depressions in the description of Earth surface processes. The preservation of depressions in the observed topographic data is a major scientific commitment in the present study. The capability to describe depressions as observed in topographic data is important to generalize existing models and to determine the circumstances under which depressions may or may not be filled.

Specific efforts have been made to retain the information content of high-resolution (1 m or less) grid DEMs when coarsening to large grids (1 km or more) is needed (e.g., Chen et al., 2012; Moretti & Orlandini, 2018; O'Donnell et al., 1999; Reed, 2003; Zhou & Chen, 2011). Existing coarsening strategies, however, are unsatisfactory as they often require DF in the observed topographic data and do not preserve essential features of land surface topography. In addition to grid DEMs, triangulated irregular networks (Ivanov et al., 2004) and contour-based flow nets have been used in terrain analysis (e.g., Dawes & Short, 1994; Maunder, 1999; Moore & Grayson, 1991; Moretti & Orlandini, 2008; Onstad & Brakensiek, 1968; O'Loughlin, 1986). The generation of triangulated irregular networks, however, is normally based on depressionless DEMs (e.g., Vivoni et al., 2004). On the basis of the pioneering studies of quantitative geomorphology by Cayley (1859) and Maxwell (1870), a flow net can be derived by partitioning the drainage basin in a number of elements, each of them being formed by an upper and lower contour segment, for the top and bottom sides of the element, and two flow lines connecting the upper and lower contour lines, for the left and right sides of the element (e.g., Moore et al., 1988; Onstad & Brakensiek, 1968; O'Loughlin, 1986). These flow nets offer, at least in principle, a series of advantages over more efficient and straightforward DEMs (e.g., gridded regular or triangulated irregular) since they explicitly reproduce the way in which water and sediment flow on the land surface under the effect of gravity. Several studies have been carried out to improve the accuracy and the degree of automation in the delineation of drainage basins and the construction of flow nets (e.g., Maunder, 1999; Moretti & Orlandini, 2008). Flow nets, however, are especially designed to describe gravity-driven processes and, in any case, a classical flow net derived using flow lines is not suited to natural landscapes because flow strips lying between flow lines continually merge or split, and the flow net has to be modified by amalgamating excessively small elements and subdividing excessively large elements (Moore & Grayson, 1991). There is therefore a need for physically meaningful descriptions of land surface topography that retain the essential information content of high-resolution grid DEMs while also

leading to terrain partitionings that are compatible with computational efficiency requirements of models for the description of Earth surface processes. The resolution of grid DEMs used to describe the land surface topography can range from 1 mm or less to 1 km or more depending on the scale and scope of the investigation. In any case, it is relevant to retain the essential topographic features observed in topographic data when these data are coarsened for computational efficiency.

The lines following the lowest part of a valley or channel (thalwegs) and the lines of intersection at the top between opposite slopes (ridges) are the essential topographic features (bases) that need to be extracted from observed topographic data and retained when terrain is partitioned. Thalwegs indicate main flow paths and depression bottoms. Ridges indicate flow divides and barriers to flow. Since depression bottoms are thalwegs and depression borders are ridges, the preservation of depressions and the preservation of thalweg and ridge network structures are equivalent requirements. The relevance of thalweg and ridge networks has been recognized in the literature (e.g., Cayley, 1859; Chang et al., 1998; Lindsay & Seibert, 2012; Maxwell, 1870; Perron et al., 2009; Rak et al., 2019; Rana, 2006; Werner, 1972, 1988; Willett et al., 2014; Zhang & Jia, 2020). Werner (1972, 1988) provided a formal analysis of channel and ridge networks as interlocked tree structures. Chang et al. (1998) proposed a program based on profile recognition and polygon-breaking algorithms to automatically extract ridge and valley axes. Lindsay and Seibert (2012) introduced a maximum branch length that is similar to the average length of the two slopelines extending from a ridge point on the opposite slopes of the ridge until they rejoin used in the present study. Endorheic basins are appropriately identified in Barnes et al. (2020, 2021). Zhang and Jia (2020) proposed a watershed merging method that connects depressions and flat areas without altering the observed topographic data. In these studies, however, exorheic and endorheic basins are not connected without altering the observed topographic data, or connections are not determined in a physically meaningful manner and the resulting channel network is not unequivocally defined. In addition, the profile recognition process used to determine the ridge network is not robustly connected to the roles played by ridges and valleys in Earth surface processes. Therefore, the extraction of physically meaningful thalweg and ridge networks from unaltered high-resolution topographic data remains a challenge. To solve this challenge, it is important that the extracted thalweg and ridge networks fully penetrate the computational domain and can be hierarchized in a physically meaningful manner so that they can eventually be pruned to inform terrain partitioning and the description of Earth surface processes at the desired level of detail. In the present study, it is shown that such physically meaningful thalweg and ridge networks can be extracted automatically from unaltered high-resolution grid DEMs, and that these networks can be represented at the desired level of detail to provide suitable bases for terrain partitioning. The methods are described in Section 2, the applicability and impact of these methods are evaluated in Section 3, the results are discussed in Section 4, and conclusions are given in Section 5.

## 2. Methods

The workflow of new terrain analysis methods based on unaltered topographic data, as compared to the workflow of existing terrain analysis methods based on grid coarsening and DF, is reported in Figure 1. Even when high-resolution grid DEMs are available, in existing terrain analysis (left-hand-side column in Figure 1), grids are often coarsened for computational efficiency and depressions are commonly filled for model simplicity (before and/or after grid coarsening) by using, for instance, the priority flood algorithm (Barnes et al., 2014). The slopline network is then extracted to inform the identification of the channel network using the D8-LTD method (Orlandini et al., 2003, 2014). A new paradigm for terrain analysis is proposed in the present study (right hand side column in Figure 1). High-resolution grid DEMs are not altered by grid coarsening or DF, but rather are used to directly extract the slopline network. Points lying on ridges (ridge points), exorheic and endorheic basins, and saddle points at which endorheic basins are filled by water and sediments and start to spill into their neighboring (exorheic or endorheic) basins (spilling saddles) are then identified based on the slopline network. Physically meaningful thalweg and ridge networks connecting exorheic and endorheic basins are finally extracted. By generating an unstructured mesh that adapts to extracted thalweg and ridge networks, the essential topographic features observed in high-resolution topographic data are preserved and the terrain is partitioned into elements having variable size, resulting in an unstructured mesh that is compatible with the computational efficiency requirements of models for the description of Earth surface processes. With existing methods, terrain partitioning is applied before the channel network is extracted. With the new algorithm proposed in this work, named LANDMARK, thalweg and ridge networks are extracted from unaltered topographic data and are used as essential topographic features (bases, or landmarks) to inform terrain partitioning. The essential theoretical

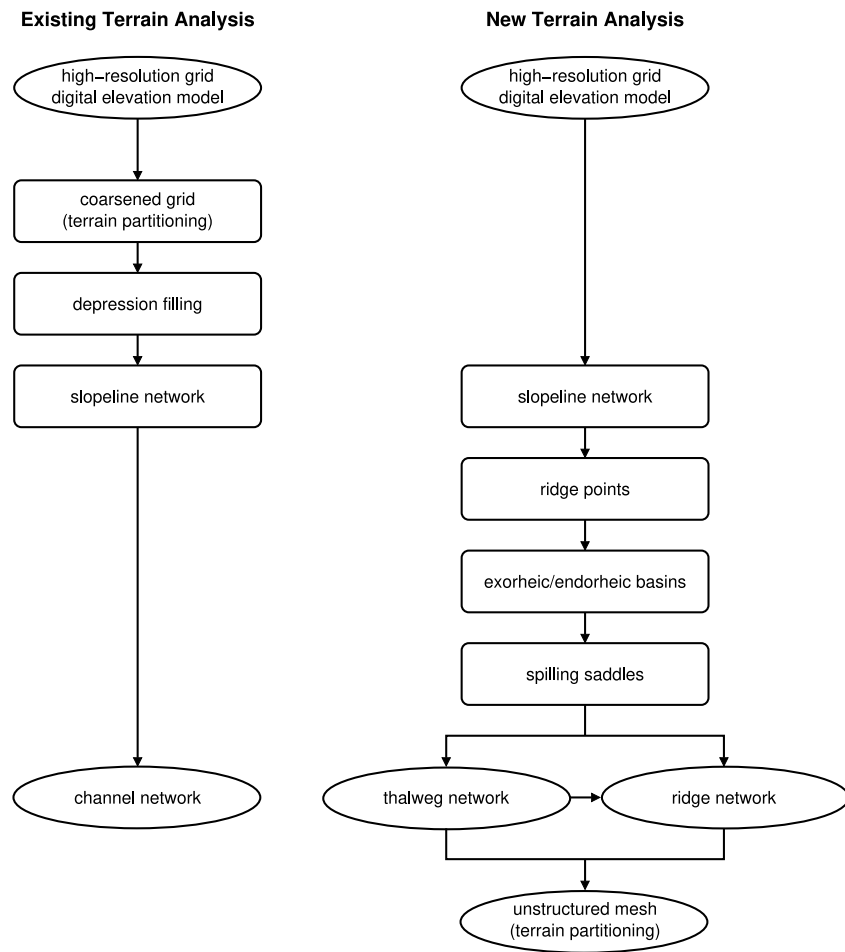


**Figure 1.** Workflows of existing terrain analysis based on grid coarsening and depression filling (left hand side column) and new terrain analysis based on unaltered topographic data (right hand side column).

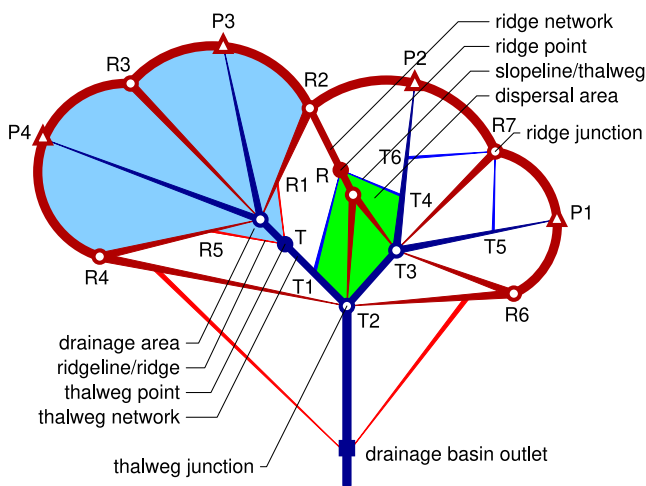


**Figure 2.** Sketch of the thalweg and ridge networks when the attention is focused on the drainage basin. The well-known concept of drainage area contributing to a given thalweg point is related to ridges of the ridge network, and the extended concept of dispersal area from a given ridge point is related to thalwegs of the thalweg network.

framework underlying the proposed methods is described in Section 2.1. The use of sloplines for the determination of ridge points and exorheic and endorheic basins is described in Section 2.2. The extraction of the thalweg network is described in Section 2.3. The determination of the ridge network is described in Section 2.4. The use of the thalweg and ridge networks as bases for terrain partitioning is shown in Section 2.5.

### 2.1. Theoretical Framework

The concepts of thalweg and ridge networks are sketched in Figure 2. The thalweg is a line following the lowest part of a valley or channel. Mathematically, thalwegs extend along sloplines (lines at right angles to the contour lines, Cayley, 1859), where the terrain has a convergent topography and a negative plan curvature (curvature of contour lines, Zevenbergen & Thorne, 1987). Physically, thalwegs are sloplines along which water and sediments concentrate from the surrounding terrain through converging sloplines under the effect of gravity. The junction between the thalwegs is denoted as a thalweg junction. A connected network of thalwegs is denoted as a thalweg network. A point of the thalweg network is denoted as a thalweg point. The ridge is a line of intersection at the top between opposite slopes. Mathematically, ridges extend along sloplines where the terrain has a divergent topography

and positive plan curvature. Physically, ridges are slopelines along which water and sediments distribute (or spread) to the surrounding terrain through divergent slopelines under the effect of gravity. The junction between the ridges is denoted as a ridge junction. A connected network of ridges is denoted as a ridge network. A point of the ridge network is denoted as a ridge point. Although both thalwegs and ridges extend along slopelines, water and sediments are collected by thalwegs due to the surrounding convergent topography and are distributed (or spread) by ridges due to the surrounding divergent topography. This distinction can be made using the term “slopline” for thalwegs and the term “ridgeline” for ridges. Mathematically, thalwegs and ridges join in saddles. However, by extracting first a fully integrated thalweg network and then identifying the related ridge network, thalweg and ridge networks can be recognized to be interlocked and interdependent tree structures as reported in Werner (1988) and sketched in Figure 2.

Any thalweg point (dark blue filled circle in Figure 2) is characterized by a drainage area (light blue area in Figure 2). The drainage area is the area contributing water and sediments to the thalweg point and the related subnetwork through gravity-driven flows occurring along slopelines. In Figure 2, the drainage area contributing to the thalweg point *T* is bordered by the ridges T-R1-R2-P3-R3-P4-R4-R5-T, and the drainage area contributing to thalweg P1-T3 is bordered by the ridges T3-R6-P1-R7-T3. Ridges belonging to the sketched ridge network are represented by dark red lines, whereas ridges extending on lateral areas are represented by red lines. The drainage area associated with a thalweg point is bounded by ridges and spatially penetrated by the thalweg subnetwork. Any ridge point (dark red filled circle in Figure 2) is characterized by a dispersal area (green area in Figure 2). The dispersal area is defined here as the area distributing water and sediments from the ridge point and the related subnetwork through gravity-driven flows occurring along slopelines. This concept extends the concept of dispersal area introduced by Martz and de Jong (1987) and Costa-Cabral and Burges (1994). In Figure 2, the dispersal area distributed from the ridge point *R* is bordered by thalwegs R-T1-T2-T3-T4-R, and the dispersal area distributed from ridge R7-T3 is bordered by the thalwegs R7-T6-T3-T5-R7. Thalwegs belonging to the sketched ridge network are represented by the dark blue lines, whereas thalwegs extending on lateral areas are represented by blue lines. The dispersal area associated with a given ridge point is bounded by thalwegs and spatially penetrated by the ridge subnetwork.

The dispersal area complements the concept of drainage area. As shown in Figure 2, the thalweg network and the related drainage areas describe the concentration (or drainage) of flows that are distributed (or spread) by the ridge network and related dispersal areas. Ridges spread and thalwegs drain gravity-driven flows along slopelines, with a different role that is connected to the divergent (positive plan curvature) or convergent (negative plan curvature) topography around these slopelines. However, within the drainage and dispersal areas, gravity-driven flows are not purely convergent or divergent. Convergent and divergent flows occur in interlocked capillary networks of thalwegs and ridges that are represented by the LANDMARK algorithm as described in Sections 2.2–2.4. Although thalwegs and ridges can be mathematically characterized in terms of plan curvature, the LANDMARK algorithm identifies them numerically using the extracted slopline network. With this modeling strategy, thalweg and ridge networks are determined in a numerically robust manner and can be hierarchized using the concepts of drainage and dispersal areas. In a similar way as the importance of a thalweg within a thalweg network is indicated by the related drainage area, the importance of a ridge within the ridge network is indicated by the related dispersal area. From the full (unpruned) thalweg network extracted in a grid DEM, pruned thalweg networks can therefore be obtained by cutting all thalwegs that have a drainage area less than a selected critical value. Similarly, from the full (unpruned) ridge network extracted in a grid DEM, pruned ridge networks can be obtained by cutting all ridges that have a dispersal area less than a selected critical value.

The average length of the two slopelines extending from a ridge point on the opposite slopes of the ridge until they rejoin is used in the present study to determine exorheic and endorheic basins. This average length is denoted as the average rejunction length and is conceptually similar to the maximum branch length introduced by Lindsay and Seibert (2012). In Figure 2, the average rejunction length associated with the ridge point *R* is the average between the two lengths of slopelines R-T1-T2 and R-T4-T3-T2 joining in T2. The area bordered by the rejunction path R-T1-T2-T3-T4-R is the dispersal area associated with the ridge point *R*. Both average rejunction lengths and dispersal areas associated with ridge points can be used to identify exorheic and endorheic basins. In the present study, the average rejunction length was used to identify exorheic and endorheic basins, whereas the dispersal area was used to characterize ridges within the ridge network. If the average rejunction length associated with a ridge point displays a finite value, then the two related slopelines extending from the ridge point on the opposite slopes of the ridge join within the considered domain and the related ridge point divides two exorheic basins. In

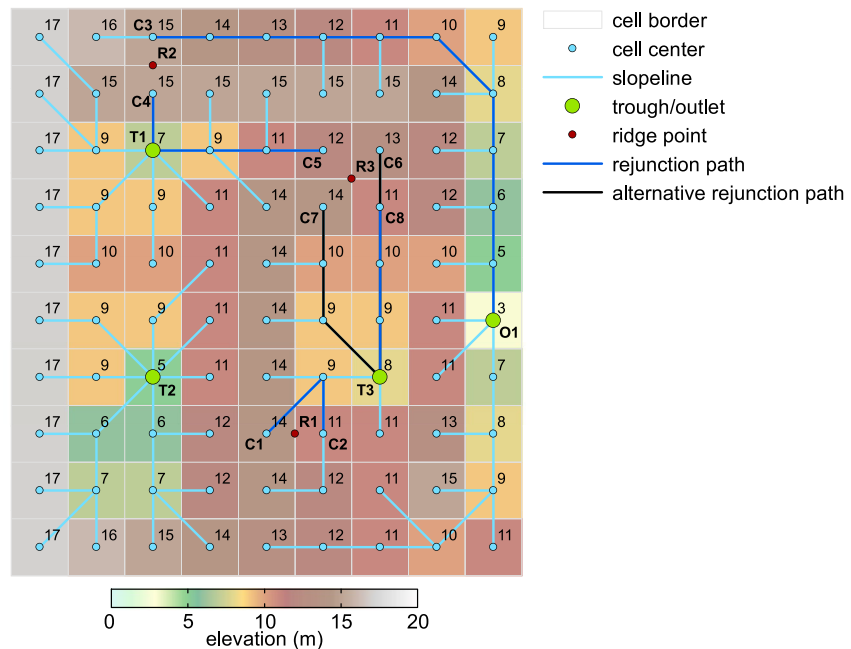


**Figure 3.** Sketch of a simple synthetic case showing the slopelines extracted from the grid digital elevation model (elevations reported close to cell centers), the endorheic basin troughs (T1–T3), and the exorheic basin outlet (O1). Relevant examples of ridge points (R1–R3) and related paths along which the average rejunction length is computed are highlighted.

Figure 2, slopelines R-T1-T2 and R-T4-T3-T2 join in T2 and R divides therefore two exorheic basins. If the average rejunction length associated with a ridge point does not display a finite value, then the two related slopelines extending from the ridge point on the opposite slopes of the ridge do not join within the considered domain and the related ridge point divides two basins, at least one of which is an endorheic basin, or two exorheic basins flowing into different outlet points along the border of the computational domain. In any case, it is possible to determine whether a basin divided by a ridge point is exorheic or endorheic.

In the thalweg network, exterior thalwegs begin at some ridge points (dark red empty triangles in Figure 2) along ridges bordering the related drainage area and connect to the thalweg network in thalweg junctions (dark blue empty circles in Figure 2). The points at which thalwegs begin may be assumed to be the uppermost ridge points or the extensions upstream of the slopelines draining the largest area. This issue is not relevant if the thalweg network is pruned, but it can be investigated in future studies. In Figure 2, for instance, thalweg P1-T3 begins at the uppermost ridge point P1 along the ridges T3-R6-P1-R7-T3 and connects to the thalweg network in the thalweg junction T3. In the ridge network, exterior ridges begin from thalweg junctions (which are the lowermost thalweg points along thalwegs bordering the related dispersal area) and connect to the ridge network in ridge junctions (dark red empty circles in Figure 2). In Figure 2, ridge T3-R7 begins at the thalweg junction T3 and connects to the ridge network in the ridge junction R7, T3 being the lowermost thalweg point of thalwegs R7-T6-T3-T5-R7 (which borders the dispersal area of R7). Mathematically, the slopline beginning from a ridge point is a ridge, but thalwegs may begin from any points lying in the neighborhood around a ridge. Similarly, the slopelines from a thalweg junction are thalwegs, but ridges may begin from any points lying in the neighborhood around a thalweg. Numerically, this issue is solved by selecting thalweg points among grid cell centers and ridge points among grid cell border midpoints and vertices as will be shown in Section 2.2, so that the thalwegs from a ridge point actually begin from the closest thalweg point and the ridges from a thalweg point actually begin from the closest ridge point.

## 2.2. Ridge Points

Slopelines, ridge points, exorheic basin outlets, and endorheic basin troughs are automatically identified in the available high-resolution grid DEM as sketched in Figure 3. Slopelines (lines reported in cyan in Figure 3) are first determined using the D8-LTD slope direction method (Orlandini et al., 2003, 2014). Observed topographic

data are not altered by applying a DF procedure. Slopelines end in cells having no neighboring draining cells. The centers of these cells are identified as endorheic basin troughs (T1, T2, and T3 in Figure 3) if the cells are internal to the domain, or exorheic basin outlets (O1 in Figure 3) if the cells are on the domain border. Inabilities to distinguish (endorheic basin) troughs and (exorheic basin) outlets are only possible for cells lying on the domain border, but certainly not for cells lying within the domain. Slopeline ends in cells lying on the domain border are considered to be exorheic basin outlets. These possible border effects do not limit the generality of the proposed methods. Disconnected slopeline networks ending in endorheic basin troughs or exorheic basin outlets are obtained.

Ridge points are identified as all grid cell border midpoints or vertices internal to the domain that are not crossed by slopelines (e.g., R1–R3 in Figure 3). Cell border midpoints and vertices lying on the domain border are not considered to be ridge points and this does not limit the generality of the proposed methods. Ridge points are associated with the outlets or troughs of the divided basins and are characterized by two essential attributes, namely the ridge point elevation and the average rejunction length of slopelines extending from the ridge point on the opposite slopes of the ridge until they join. Ridge points that are grid cell border midpoints have two closest cell centers (for instance, in Figure 3, C1 and C2 are the closest cell centers to R1), whereas ridge points that are cell vertices have four closest cell centers (for instance, C5–C8 are the closest cell centers to R3). The ridge point elevation is computed as the maximum elevation among those of the closest cell centers (for instance, 14 m for R1, 15 m for R2, and 14 m for R3 in Figure 3). The average rejunction length is half the length of the closed path given by two slopelines originating from the ridge point's closest cell centers, extending on the opposite slopes of the ridge, and ending where these slopelines rejoin. If the two slopelines do not join within the considered domain, the average rejunction length is conventionally set equal to a “huge length” (HL) that cannot be reached using computed average rejunction lengths (e.g.,  $10^{12}$  m). If the ridge point is a cell edge midpoint, then at least one pair of divided cell centers exists (for instance, R1 divides C1 from C2 in Figure 3). If the ridge point is a cell vertex, then two pairs of divided cell centers exist (for instance, R3 divides C5 from C8 and C6 from C7 in Figure 3). The average rejunction length associated with a ridge point lying on a cell edge midpoint is computed along the slopelines originating on the opposite slopes of the ridge from the closest cell centers to the ridge point if these slopelines join (for instance, average rejunction length along the path highlighted in blue from C1 and C2 in Figure 3) or is set equal to HL if these slopelines do not join (for instance, average rejunction length from C3 and C4 in Figure 3). The average rejunction length associated with the ridge point lying in a cell vertex is computed as the maximum of the two average rejunction lengths computed over the two pairs of closest cell centers (for instance, the average rejunction length associated to R3 is set equal to HL in Figure 3). Ridge points are used to determine the thalweg and ridge networks as described in Sections 2.3 and 2.4, respectively. The pseudocode for the determination of ridge points is reported in Appendix A.

### 2.3. Thalweg Network

The thalweg network is obtained by combining the slopeline network extracted from the observed topographic data (with depressions) and additional thalweg elements connecting exorheic and endorheic basins as sketched in Figure 4. An endorheic basin is connected to an exorheic basin or to another endorheic basin through a saddle that is denoted in the present study as a spilling saddle. To identify the spilling saddles from endorheic basins, only those ridge points displaying an average rejunction length equal to HL are considered (largest red circles in Figure 4). These ridge points separate (exorheic or endorheic) basins having different outlets or troughs. Since ridge points are associated with the outlets or troughs of the divided basins as reported in Section 2.2, it is possible to identify among all the ridge points separating two given exorheic or endorheic basins having different outlets or troughs the one displaying the lowest elevation, that is considered to be the lowest saddle between the two divided basins (large red and blue circles in Figure 4). In order to identify the spilling saddles connecting an endorheic basin to an exorheic or another endorheic basin, these lowest saddles are processed in order of increasing elevation using a two-step nested procedure.

In the first step, for each saddle processed in order of increasing elevation, it is tested whether the saddle divides an endorheic basin from an exorheic basin (for instance, S1 in Figure 4) or rather divides two endorheic basins. In the former case, since the saddles processed are in order of increasing elevation, the saddle is considered to be a spilling saddle and the endorheic basin trough is connected to the exorheic basin outlet through a spilling saddle path (for instance, path T3-S1-O1 in Figure 4). The connected endorheic basin is marked as visited and conceptually classified as a new portion of the draining exorheic basin. In the second step, inside the connected basin, nested endorheic basins are sought and connected. This is implemented by seeking among all the saddles existing in the

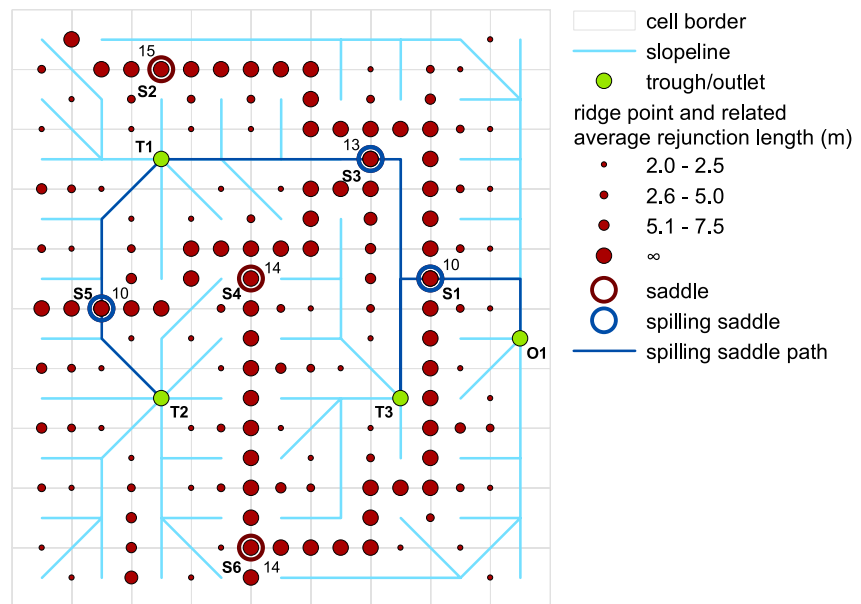


**Figure 4.** Sketch of the simple synthetic case introduced in Figure 3, where all the ridge points are classified using the average rejunction length spilling saddles from endorheic basins (S1, S3, and S5) are identified, and exorheic and endorheic basins are connected.

connected basin those displaying a lower elevation than the spilling saddle elevation (for instance, no such saddles are found in the connected basin having trough T3 as S3 and S4 display a higher elevation than S1 in Figure 4, being S6 a saddle dividing the exorheic basin with outlet O1 from the endorheic basin with trough T2). It is noted that all the saddles considered in the second step are skipped in the first step because they divide two endorheic basins (and not an endorheic basin from an exorheic basin). The saddles found in the connected basin are sorted in order of increasing elevation and the second step is iteratively applied only to these saddles. In the second step, a connected endorheic basin is marked as visited and conceptually classified as a new portion of the draining exorheic basin.

Two essential points of the two-step nested procedure are as follows: (a) saddles are processed in order of increasing elevation and (b) an endorheic basin is marked as visited and conceptually classified as a new portion of the draining exorheic basin immediately after it is connected. A two-step procedure is needed to ensure that each endorheic basin is connected to an exorheic basin directly (first step) or through other endorheic basins (second step) through the saddles displaying the lowest elevations. In Figure 4, for instance, the saddle S3 is processed by the first step as it divides the endorheic basin having trough T1 from the endorheic basin having trough T3 that has already been connected and is now conceptually classified as a new portion of the draining exorheic basin having outlet O1. S3 is found to be the spilling saddle of the endorheic basin having trough T1. This endorheic basin is connected to O1 though the spilling saddle path T1-S3-S1-O1 and is marked as visited so that it can now be conceptually classified as a new portion of the draining exorheic basin having outlet O1. In the second step, the saddle S5 is found to have a lower elevation (10 m) than the elevation of the spilling saddle S3 (13 m). Since S5 divides the basin having trough T1 that has been conceptually classified as a new portion of the draining exorheic basin having outlet O1 and the endorheic basin having trough T2, S5 is considered to be the spilling saddle of the nested endorheic basin having trough T2. This nested endorheic basin is connected to O1 though the spilling saddle path T2-S5-T1-S3-S1-O1 and is conceptually classified as a new portion of the draining exorheic basin having outlet O1. Slope lines and spilling saddle paths form the thalweg network. The full thalweg network extracted from the high-resolution grid DEM can be pruned by setting a critical drainage area for the thalweg representation  $A_c$ . The pseudocode for the determination of the thalweg network is reported in Appendix B.

#### 2.4. Ridge Network

The ridge network is formed by ridgelines. Ridgelines are lines obtained by connecting ridge points. In order to determine the ridge network, it is essential that ridgelines are identified and ridgeline junctions are solved in an ordered manner as sketched in Figure 5. Ridgeline starting points are sought among ridge points lying close to



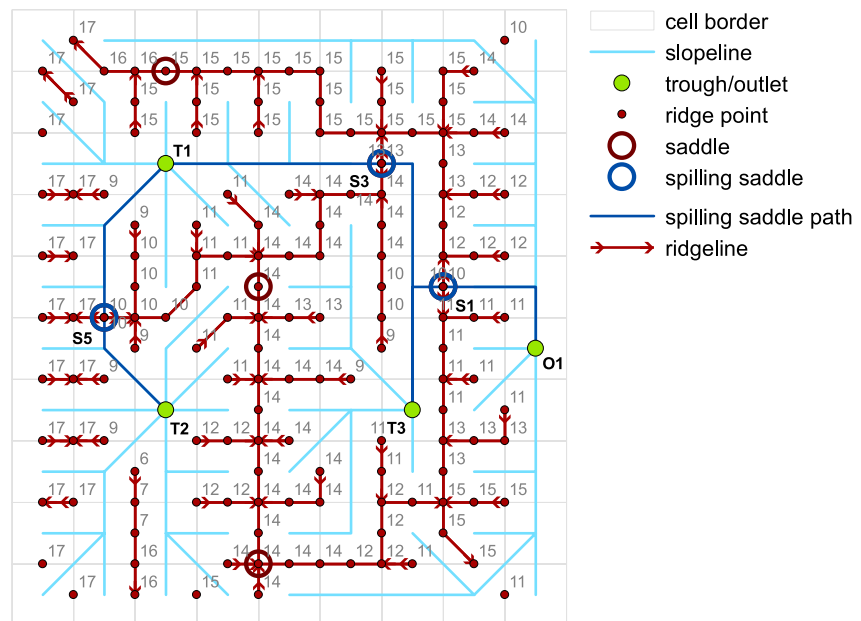


**Figure 5.** Sketch of the simple synthetic case introduced in Figure 3, where ridgelines are identified from starting points lying close to thalweg junctions and spilling saddles to obtain the ridge network.

thalweg junctions and spilling saddles from endorheic basins, and are considered in order of increasing elevation. From these starting points, ridgelines are identified and ridgeline junctions are solved on the basis of relationships between neighboring ridge points. As shown in Figure 5, each ridge point has at least one neighboring ridge point. Three cases are possible. First, the ridge point has only one neighboring ridge point. This indicates that the ridge point is located near a thalweg junction where a ridgeline originates. Outward arrows from the ridge points having one neighbor indicate these cases in Figure 5. Second, the ridge point has two neighboring ridge points. This indicates that the ridge point is neither a ridgeline starting point nor a ridgeline junction (Figure 5). Third, the ridge point has three or four neighboring ridge points. This indicates that the ridge point is a ridgeline junction (Figure 5). Ridge points identified as spilling saddles need to be processed in a specific way so that they can be ascribed to the first case and not to the second one. In ridge points identified as spilling saddles, slope lines are conceptually connected to form a tree thalweg network (Section 2.3) and the ridgeline is conceptually disconnected in such a way that a tree ridge network is obtained. The disconnection of the ridgeline in a ridge point identified as a spilling saddle is implemented by conceptually splitting the ridge point into two ancillary ridge points from which two ridgelines originate on opposite directions (for instance, S1, S3, and S5 in Figure 5). In this way, all ridgelines begin from ridgelines starting points lying close to a junction in the thalweg network or in a spilling saddle from an endorheic basin and end when another ridgeline or a ridgeline peak is met.

A two-step nested procedure is needed to identify ridgelines and solve ridgeline junctions along ridge profiles that do not display monotonic variations in elevation but rather display local minima (saddles) and maxima (peaks). Ridgelines are identified and extended by considering for each ridge point the number of unconnected neighboring ridge points (URP), namely the number of neighboring ridge points that are not connected to any ridgeline yet. In the first step, ridge points are processed in order of increasing elevation. Only ridge points having one unconnected neighboring ridge point ( $URP = 1$ ) are considered, whereas ridge points having more than one unconnected neighboring ridge point ( $URP > 1$ ) are temporarily skipped and left to be reconsidered by the second step. When a ridge point having one unconnected neighboring ridge point ( $URP = 1$ ) is found and it does not belong to any ridgeline already delineated, this ridge point is marked as a ridgeline starting point and its number of URP decreases by 1 ( $URP = 0$ ). The neighboring ridge point is marked as the second ridge point of the ridgeline and its number of URP is decreased by 1 (for instance, URP is decreased from 2 to 1). When a ridge point having one unconnected neighboring ridge point ( $URP = 1$ ) is found and it belongs to a ridgeline already delineated, two cases are possible. First, if this ridge point originally had only two URP, then it is neither a ridgeline starting point nor a ridgeline junction and it has already been considered

only once. Second, if this ridge point originally had three or four URP, then it is a ridgeline junction and it has already been considered and connected to two or three different joined ridgelines, respectively, with URP decreased by 1 every time the junction ridge point has been connected to a joined ridgeline. In both cases the identification of the ridgeline continues in the direction of the only unconnected neighboring ridge point left, this neighboring ridge point is marked as a ridge point belonging to a ridgeline, and its number of URP is decreased by 1. If the elevation of this neighboring ridge point added to the ridgeline is less than or equal to the elevation of the connecting ridge point, then the connecting ridge point is marked as a maximum and the second step is started.

In the second step, to overcome the problem of local minima, URP having elevation less than or equal to the elevation of the last connecting ridge point considered in the first step (the ridge point having maximum elevation) are progressively connected to the ridgeline. Ridge points considered in the second step have already been visited in the first step because they have lower elevation than the elevation of the last connecting ridge point considered in the first step (the ridge point having maximum elevation), but they were found to have more than one unconnected neighboring ridge point ( $URP > 1$ ) and therefore they were not connected to any ridgeline. The identification of the ridgeline continues in the second step until a ridge point having elevation greater than the elevation of the last connecting ridge point considered in the first step (the ridge point having maximum elevation) is found. This ridge point is not connected to the ridgeline in the second step, but rather left to be considered by following the phases of the first step. If, in the second phase, a connected ridge point displays more than one unconnected neighboring ridge point ( $URP > 1$ ) even after its URP is decreased by 1, then this ridge point is recognized to be a junction with much unconnected neighboring ridge point left, and phase two is stopped. This junction will be reached by other ridgelines identified from ridge points having higher elevations that have not been considered yet through a combination of first and second phases, and its URP will be decreased by 1 every time a ridgeline joins it. The identification of the ridgeline from this junction will continue only when its number of neighboring ridge points is found to be 1 in the direction of the only neighboring ridge point left. The procedure calls the first and second steps one after the other and ends when the highest peak of the considered geographical area is reached, that is, when the root of the ridge network having a tree structure is recognized. While step one processes ridge points in order of increasing elevation going from one location to another within the geographical area, the second step processes the ridge points along a well-defined ridgeline by solving local minima and reconsidering ridge points that were skipped by the first step. Ridgelines form the ridge network. The full ridge network extracted from the high-resolution grid DEM can be pruned by considering only ridges associated with thalwegs with drainage area greater than or equal to the critical drainage area for thalweg representation  $A_c$ , or directly from the full ridge network by setting a critical dispersal area for ridge representation  $S_c$ . The pseudocode for the determination of the ridge network is reported in Appendix C.

## 2.5. Terrain Partitioning

The obtained thalweg and ridge networks are used as bases for the determination of physically meaningful terrain partitionings as sketched in Figure 6. This partitioning is described by an unstructured mesh obtained using the domain boundary, the thalweg network, and the ridge network as breaklines. A breakline is a line used to connect data representing a distinct land surface feature, like a domain boundary, a ridgeline, or a flowline of a ditch or stream. The mesh generator included in the Hydrologic Engineering Center (HEC) River Analysis System (RAS) developed by the US Army Corps of Engineers was used in the present study (Hydrologic Engineering Center, 2016, 2022). Breaklines are incorporated by the HEC-RAS mesh generator in accordance with an assigned point spacing. When a breakline is defined, the HEC-RAS mesh generator seeks a Voronoi tessellation that follows the breakline by placing the polygon edges coincident with the breakline segments. This ensures that the features in the terrain are accurately depicted in the computational mesh by forcing those cell facets to have the elevation values of the thalwegs and ridges. Far from assigned breaklines, the Voronoi tessellation is unconstrained and therefore gives a regular mesh. The Voronoi polygons given by the HEC-RAS mesh generator are the elements of the unstructured computational mesh that is used to describe surface flow propagation as reported in Section 3.2. Results obtained from the HEC-RAS mesh generator are generally satisfactory and can be made as accurate as desired by applying some mesh refinement in points when Voronoi polygon edges are not found to adapt perfectly to the assigned breaklines. The problem of determining the optimal Voronoi tessellation that adapts to assigned thalweg and ridge networks is beyond the scope of the present paper, but it certainly deserves to be addressed in a future specific research effort.

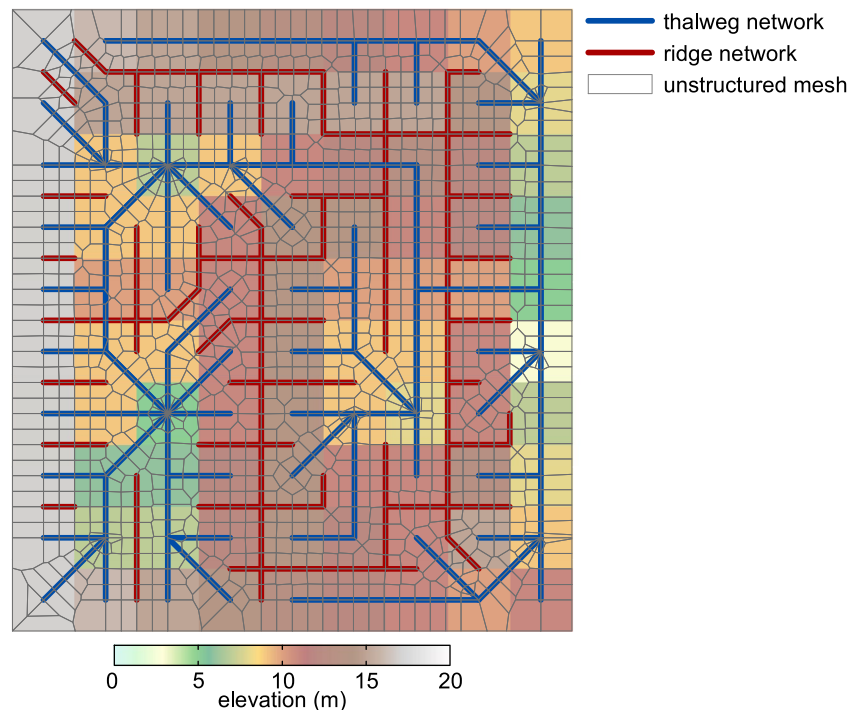


**Figure 6.** Sketch of the simple synthetic case introduced in Figure 3, where terrain is partitioned in a physically meaningful manner by generating an unstructured mesh that adapts to the thalweg and ridge networks.

### 3. Evaluation

The ability of the LANDMARK algorithm to automatically extract the thalweg and ridge networks from high-resolution grid DEMs and the impact of preserving land surface depressions are evaluated over a mountainous terrain located inside or close to the Cordevole River drainage basin (eastern Italian Alps) as described in Section 3.1. The benefits of unstructured computational meshes based on thalweg and ridge networks in surface flow propagation modeling are shown in Section 3.2 by considering the flood event that occurred in the lowland region between the Secchia and Panaro Rivers (Po Valley, Italy) on 19 January 2014 (Orlandini et al., 2015).

#### 3.1. Highlands

The mountainous terrain located inside or close to the Cordevole River drainage basin is considered to be a representative example of a complex highland in near-natural conditions. This terrain is shown in Figure 7. The Cordevole River drainage basin is located in the eastern Italian Alps near the town of Belluno and has an extension of approximately 701 km<sup>2</sup>. The centroid of the drainage basin has latitude 46°21'33.92"N and longitude 11°58'43.69"E. The drainage basin elevation ranges from 360 to 3,343 m above sea level (asl) with an average elevation of 1,653 m asl. The geological formations are mainly limestones, dolomite, marl, and sandstones that characterize the main ranges where jagged peaks and rock faces hundreds of meters high rise from forests and grasslands. The complex geology provides constraint for the formation of the channel network, that may extend in many cases along wide valleys followed in a downstream direction by narrow canyons as reported in Figure 7. A complex ridge network is observed as a result of the competition between tectonic uplift and erosion. Specific attention is focused on a portion of the Pala Group plateau (inset A of Figures 7 and 8 and Figure S3 in Supporting Information S1), where a complex system of nested endorheic basins exists, and on the Rio Andraz drainage basin (inset B of Figures 7 and 9), where a complex system of ridges and valleys exists.

High-resolution (1-m or 2.5-m) DEMs generated from lidar surveys are available for the Cordevole River drainage basin and the surrounding geographical area. A 1-m DEM is available for most of the considered geographical areas as a combination of three sources. A first portion of the 1-m DEM was generated from a lidar survey carried out in 2017 by Regione del Veneto (Venice, Italy). The related density of survey points is greater than 1.5 points/m<sup>2</sup>.

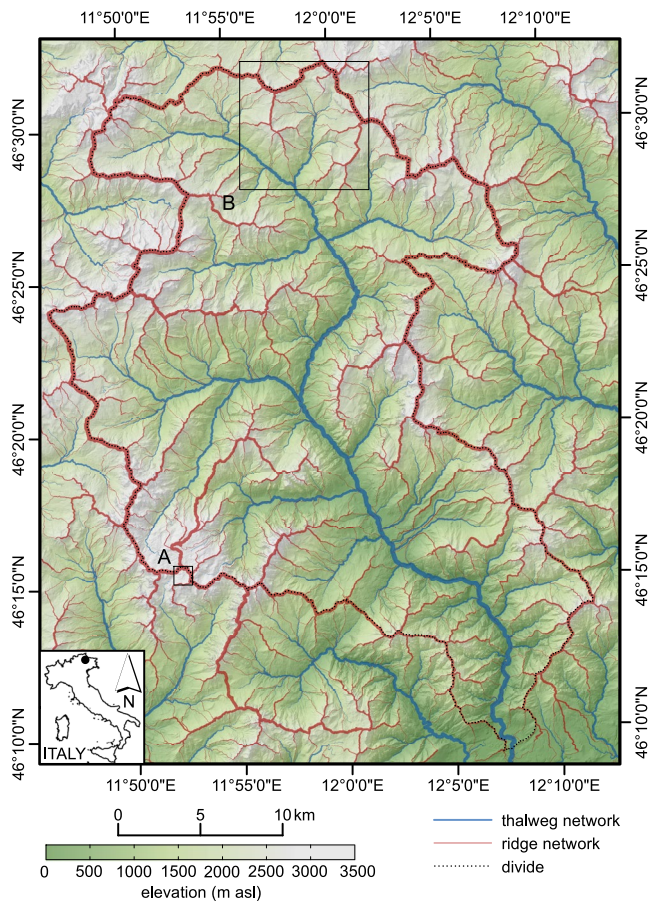


**Figure 7.** Thalweg and ridge networks extracted from the 5-m digital elevation model of the Cordevole River drainage basin (eastern Italian Alps) by setting the critical drainage area for thalweg representation  $A_c = 10^6 \text{ m}^2$ . The inset A identifies the area considered in Figure 8 and Figure S1 in Supporting Information S1. The inset B identifies the area considered in Figure 9. Thalweg and ridgeline thicknesses increase with the drainage area and the dispersal area, respectively.

The related DEM planimetric and vertical accuracies were both estimated to be lower than 15 cm. A second portion of the 1-m DEM was generated from a lidar survey carried out in 2008–2015 as part of the Not-ordinary Plan of Environmental Remote Sensing of the Ministero dell’Ambiente, della Tutela del Territorio e del Mare (Rome, Italy). The related density of survey points is greater than  $1.5 \text{ points/m}^2$ . The related DEM vertical accuracy was estimated to be lower than 15 cm and the planimetric accuracy was estimated to be lower than 30 cm (Di Martire et al., 2017). A third portion of the 1-m DEM was generated from a lidar survey carried out in 2006–2018 by the Provincia Autonoma di Trento (Trento, Italy). The related density of survey points is greater than  $1.28 \text{ points/m}^2$ . The related DEM vertical accuracy was estimated to be lower than 15 cm and the planimetric accuracy was estimated to be lower than 90 cm. The 2.5-m DEM was generated from a lidar survey carried out in 2006 by Provincia Autonoma di Bolzano (Bolzano, Italy). The density of survey points is greater than  $0.32 \text{ points/m}^2$ . The related DEM vertical accuracy was estimated to be lower than 40 cm for terrain elevations less than or equal to 2,000 m asl and 55 cm for terrain elevations greater than 2,000 m asl. While 1-m and 2.5-m topographic data were combined to obtain a coarsened 5-m DEM in order to handle the entire area shown in Figure 7, this coarsening was not needed to handle the smaller portion shown in Figure 8, where an accurate 1-m DEM was available.

The results obtained from the LANDMARK algorithm for the Cordevole drainage basin are reported in Figure 7. Results obtained for the complex area framed by inset A of Figure 7 are detailed in Figure 8. Results obtained from traditional terrain analysis methods for the same area are shown in Figure S1 in Supporting Information S1. The terrain partitioning obtained by considering the thalweg and ridge networks as bases is shown in Figure 9 for the area framed by inset B of Figure 7. Figures 7–9, and Figure S1 in Supporting Information S1 do not show the full thalweg and ridge networks obtained from high-resolution grid DEMs, but rather show pruned thalweg and ridge networks capturing the desired level of detail. Thalweg networks are pruned in the present study by considering only those thalwegs having a drainage area greater than or equal to a critical drainage area for thalweg representation  $A_c$ , in a similar way as often performed for channel networks (e.g., Orlandini et al., 2011). The critical drainage area for thalweg representation  $A_c$  is set equal to  $10^6 \text{ m}^2$  for Figures 7 and 9, and  $5,000 \text{ m}^2$  for Figure 8 and

Figure S1 in Supporting Information S1. Ridge networks can be pruned in different ways. The ridge networks shown in Figures 7 and 9 are generated from thalweg junctions in the pruned thalweg networks. Ridges reported in Figure 8 are generated from spilling saddles and are those needed to illustrate the borders of selected endorheic basins having area greater than or equal to  $500 \text{ m}^2$ . A pruned ridge network can also be obtained directly from the full ridge network extracted from the best available high-resolution grid DEM by selecting only those ridges displaying a dispersal area greater than or equal to a critical dispersal area for ridge representation  $S_c$  as will be reported in Section 3.2. Thalweg networks obtained by selecting critical drainage area for thalweg representation  $A_c$  equal to  $10^4$ ,  $10^6$ , and  $10^8 \text{ m}^2$  and related ridge networks generated from thalweg junctions are shown in Figures S2 and S3 in Supporting Information S1, respectively, to illustrate how the degree of spatial penetration of thalweg and ridge networks can be varied.

Thalweg and ridge networks can be ordered as proposed by Horton (1945) for the channel network (Leopold et al., 1964, p. 134). For ridges, this requires that the ridge network is fully represented over a sufficiently wide geographical area (and not over a single drainage basin) and that its highest peak is considered as the ridge network root. Alternatively, physically meaningful hierarchization of thalwegs and ridges is obtained by considering the related drainage area and dispersal area for each thalweg point and ridge point, respectively, as reported in Figures 7–9. Note that the pruning and hierarchization processes may both be based on the drainage area or dispersal area but are separate logical steps. Pruning is used to set the degree of spatial penetration of

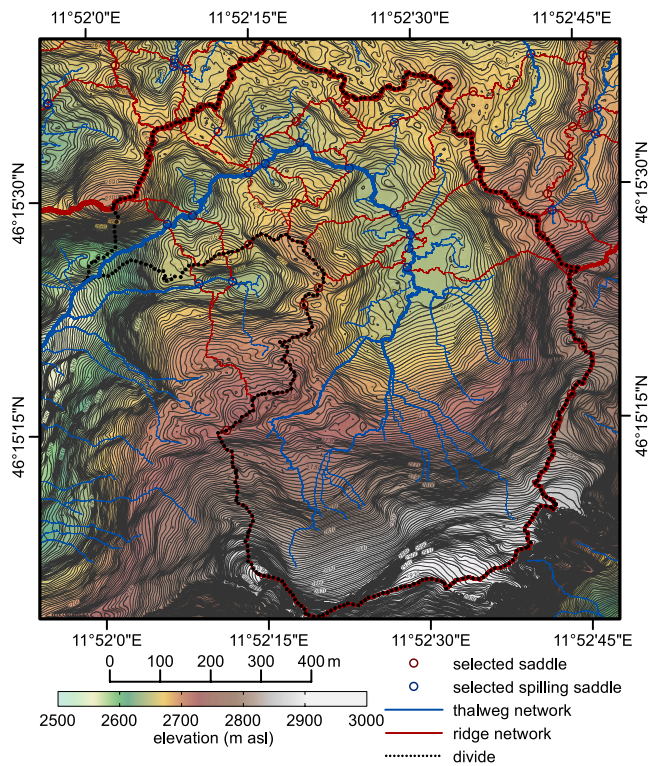


**Figure 8.** Thalweg network extracted from the 1-m digital elevation model of the Pala Group plateau located close to the Cordevole River drainage basin (eastern Italian Alps, inset A in Figure 7) by setting  $A_c = 5,000 \text{ m}^2$ . Only ridgelines delimiting endorheic basins and related saddles and spilling saddles lying along these ridgelines are reported. For clarity of representation, only endorheic basins that have an area greater than or equal to  $500 \text{ m}^2$  are considered. Thalweg and ridgeline tackiness increases with the drainage area and the dispersal area, respectively.

the thalweg and ridge networks and the detail representation of the terrain. Thalweg and ridge network hierarchizations are applied to evaluate the relative importance of thalwegs and ridges within the considered full (unpruned) or pruned networks. The improvement in the description of land surface topography due to the preservation of land surface depressions is evaluated by performing a Horton analysis of thalweg networks obtained in the two cases where LANDMARK or DF algorithms are applied. Results obtained for the Cordevole River drainage basin highlighted in Figure 7 are reported in Figures 10 and 11. High-resolution topographic data are obtained from the 5-m grid DEM of the Cordevole drainage basins. The priority flood algorithm is used to perform DF (Barnes et al., 2014), and the D8-LTD slope direction method is used to determine the slopline networks of both unaltered and altered topographic data (Orlandini et al., 2003, 2014). Elements of the thalweg network (thalwegs) are ordered using the Horton system. The number of thalwegs  $N$  having Horton order  $\omega$  is plotted in Figure 10a. The maximum order  $\omega$  is 12 when both LANDMARK and DF algorithms are applied. The mean DF depth  $D_m$  in the subbasins contributing to the thalwegs having order  $\omega$  is plotted in Figure 10b. The mean drainage area  $A_m$  contributing to thalwegs having order  $\omega$  is plotted in Figure 10c, whereas the mean filling volume  $V_m$  applied by the DF algorithm in the subbasins contributing to the thalwegs having order  $\omega$  is plotted in Figure 10d. Total drainage area  $A_t$  and total filling volume  $V_t$  computed across all the subbasins contributing to thalwegs having order  $\omega$  are plotted in Figures 10e and 10f, respectively. For each order  $\omega$ ,  $A_m = A_t/N$ ,  $V_m = V_t/N$ , and  $D_m$  can either be obtained as  $V_m/A_m$  or  $V_t/A_t$ . Similar results are obtained for the drainage basins highlighted in Figures 8 and 9 as reported in Figures S4 and S5 in Supporting Information S1, respectively.

The total filling volumes  $V_t$  in subbasins drained by thalwegs having variable Horton order  $\omega$  are shown in Figure 11 for the drainage basins highlighted in Figure 7 (Figure 11a), Figure 8 (Figure 11b), and Figure 9 (Figure 11c). Each bar reports the partial contributions of subbasins having orders less than or equal to  $\omega$  (colors indicated in the legend) that drain directly into the thalweg having order  $\omega$  and the total filling volume over all the subbasins having

order  $\omega$  (bar length). Partial contributions of subbasins having order  $\omega$  are due to grid cells crossed by the thalweg having order  $\omega$ . The data plotted in Figures 11a–c are reported in Tables S1–S3 in Supporting Information S1, respectively. For instance, in all plots of Figure 11, the navy bar associated with  $\omega = 1$  gives the total filling volume over all the subbasins having order 1 (and, clearly, there are no subbasins having order less than 1). The red bar associated with  $\omega = 2$  gives the total filling volume over all the subbasins having order 2, and insignificant contributions from subbasins having order 1 are found within the subbasins having order 2. The turquoise bar associated with  $\omega = 3$  gives the total filling volume over all the subbasins having order 3, and little contributions from subbasins having orders 1 and 2 are found within the subbasins having order 3. A similar analysis performed in terms of the number of thalwegs  $N$  having Horton order  $\omega$  is shown in Figure S6 in Supporting Information S1.

### 3.2. Lowlands

The flood plain region located along the Po River valley, between the Secchia and Panaro Rivers, near the town of Modena, Italy, is considered to be a representative example of a lowland that is significantly altered by man-made topographic structures. This region was flooded in January 2014 after a levee failure occurred along the Secchia River as reported by Orlandini et al. (2015, Figure 1). The location of the levee failure has latitude  $44^\circ 41' 57.85'' \text{N}$  and longitude  $10^\circ 56' 41.68'' \text{E}$ . The extent of the flooded area was approximately  $52 \text{ km}^2$ . The water volume released from the Secchia River to the surrounding plain was about  $36 \times 10^6 \text{ m}^3$  with a peak flow discharge of about  $434 \text{ m}^3 \text{ s}^{-1}$ . The terrain elevation in the computational domain selected to describe the flood event ranges from 10 to 35 m asl with an average elevation of 20 m asl. Although the terrain is apparently flat, natural and man-made depressions and ridges actually exist as indicated by the 1-m DEM generated from the lidar survey

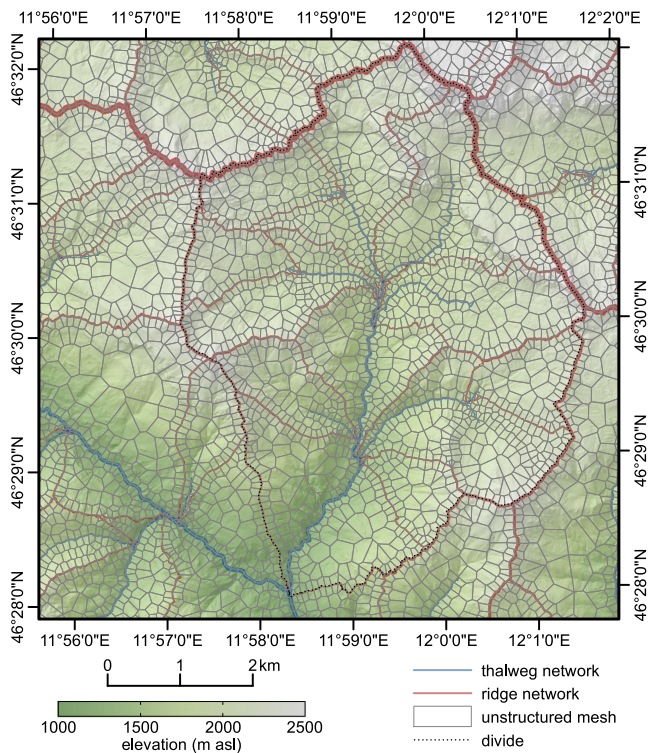


**Figure 9.** Terrain partitioning of the Rio Andraz drainage basin located inside the Cordevole River drainage basin (eastern Italian Alps, inset B in Figure 7) obtained using an unstructured mesh that adapts to the thalweg and ridge networks extracted through the LANDMARK algorithm by setting  $A_c = 10^6 \text{ m}^2$ . Thalweg and ridgeline thicknesses increase with the drainage area and the dispersal area, respectively.

carried out in 2008–2015 as part of the Not-ordinary Plan of Environmental Remote Sensing of the Ministero dell’Ambiente, della Tutela del Territorio e del Mare (Rome, Italy). The density of survey points is greater than  $1.5 \text{ points/m}^2$ . The related DEM vertical accuracy was estimated to be lower than 15 cm and the planimetric accuracy was estimated to be lower than 30 cm (Di Martire et al., 2017).

An accurate and computationally efficient description of surface flow propagation across the considered lowland terrain is obtained using the HEC-RAS 2D flood inundation model in combination with an unstructured mesh that adapts to the ridge network obtained from the LANDMARK algorithm (Hydrologic Engineering Center, 2016). The HEC-RAS 2D flood inundation model numerically solves the 2D unsteady flow equations, also known as shallow water equations (Hydrologic Engineering Center, 2020, Chapter 6, p. 3). Relevant ridges including levee, road, and railway embankments are automatically extracted from the 1-m DEM describing the land surface topography using the LANDMARK algorithm as described in Sections 2.2–2.4 and setting the critical dispersal area for ridge representation  $S_c$  equal to  $10^4 \text{ m}^2$ . An unstructured mesh that adapts to the extracted ridges is then obtained as described in Section 2.5 and shown in Figure 12. The 1-m DEM describing the land surface topography is fully assimilated by HEC-RAS 2D along the facets of mesh elements and is used to determine the distribution of surface water storage within the mesh elements (Hydrologic Engineering Center, 2022, p. 201). Ridges extracted by the LANDMARK algorithm act in HEC-RAS 2D as barriers to flow if they are set as breaklines and aligned to the mesh element facets. If extracted ridges are not aligned to the mesh element facets, they only affect the distribution of surface water storage within the mesh elements. Simulation results obtained by using an unstructured mesh based on the LANDMARK algorithm are reported in Figure 12. These results are corroborated by observations such as those shown in Figure 13. To show the relevance of the LANDMARK algorithm to flood inundation modeling, the flood event reported in Figure 12 is also simulated using an

unstructured mesh based on ridges delineated manually (Figure S7 in Supporting Information S1), and by using a regular grid having resolution of 10 m (Figure S8 in Supporting Information S1). Flooded areas obtained using an unstructured mesh based on ridges extracted automatically are similar to those obtained using an unstructured mesh based on ridges delineated manually and are significantly more accurate than those obtained using a 10-m regular grid (Figures 12 and 13, Figures S7, and S8 in Supporting Information S1). With the unstructured mesh based on the LANDMARK algorithm, the wall-clock time required for simulating a 6-day flood event over an area of  $215 \text{ km}^2$  (81,538 mesh elements) is 37 min 41 s with a workstation having an Intel Xeon E5-2687W v3 @ 3.10 GHz CPU and 128 GB RAM. With a 10-m regular grid, the wall-clock time required for simulating a 6-day flood event over an area of  $161 \text{ km}^2$  (1,619,820 grid cells) is 17 hr 28 min 50 s with the same workstation.

#### 4. Discussion

The LANDMARK algorithm described in Section 2 can process complex topographic structures such as canyons, ridges, saddles, peaks, and nested systems of exorheic and endorheic basins in a fully automated manner to yield physically meaningful thalweg and ridge networks (Figures 7–9). The thalweg network is identified by integrating the slopline network obtained from the observed topographic data with thalwegs connecting exorheic and endorheic basins through the spilling saddles (Section 2.3). Ridge points are identified immediately after extraction of the slopline network from high-resolution grid DEMs. As shown in Figure 4, all the grid cell border midpoints and vertices that are not crossed by a slopline are considered to be ridge points. Exorheic basins and related outlets, endorheic basins and related troughs, and ridge points are identified from the slopline network, as described in Section 2.2 and reported in Figures 3 and 4, by using as an essential ridge point attribute the average rejunction length of the sloplines extending from ridge points on the opposite slopes of the ridge until they join. As reported in Figure 4, ridge points displaying an average rejunction length equal to the fixed HL are those

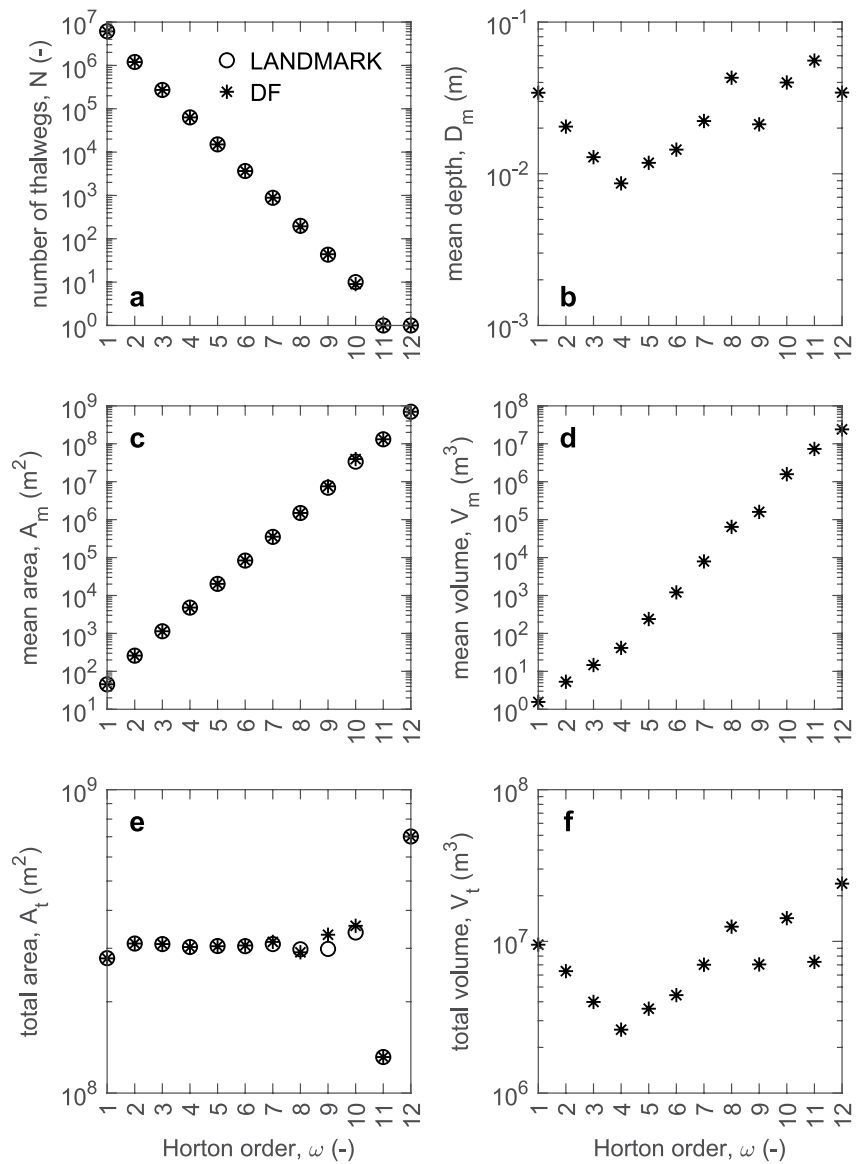


**Figure 10.** Horton analysis of thalweg networks obtained for the Cordevole River drainage basin after LANDMARK or depression filling (DF) algorithms are applied. For each Horton order  $\omega$ , the number of thalwegs  $N$ , mean filling depth  $D_m$ , mean drainage area  $A_m$ , mean filling volume  $V_m$ , total drainage area  $A_t$ , and total filling volume  $V_t$  is plotted. Results obtained after the LANDMARK (empty circles) and DF (asterisks) algorithms are compared in (a), (c), and (e). Results obtained after depression filling only are shown in (b), (d), and (f), as no DF is applied by the LANDMARK algorithm.

dividing unconnected exorheic basins or those spilling saddles dividing an endorheic basin from an endorheic or exorheic basin. In order to form a physically meaningful connected system of exorheic and endorheic basins, spilling saddles are considered in order of increasing elevation. When a spilling saddle separating an endorheic basin from an exorheic basin is found, the endorheic basin is connected to the exorheic basin. The ridge point identifying the spilling saddle is split into two ancillary ridge points and a thalweg is introduced to connect the basins. The spilling saddle is crossed by the thalweg network and includes two ancillary ridge points from which ridgelines can extend on the opposite sides of the connecting thalweg (Figure 9). The connected endorheic basin becomes a new part of the draining exorheic basin. In case there are nested endorheic basins within the connected endorheic basin, these nested endorheic basins are processed by considering the related spilling saddles in order of increasing elevation and new connections are recursively defined in the same way as reported above. This procedure makes it possible to solve any complex system of nested exorheic and endorheic basins as shown in Figure 8.

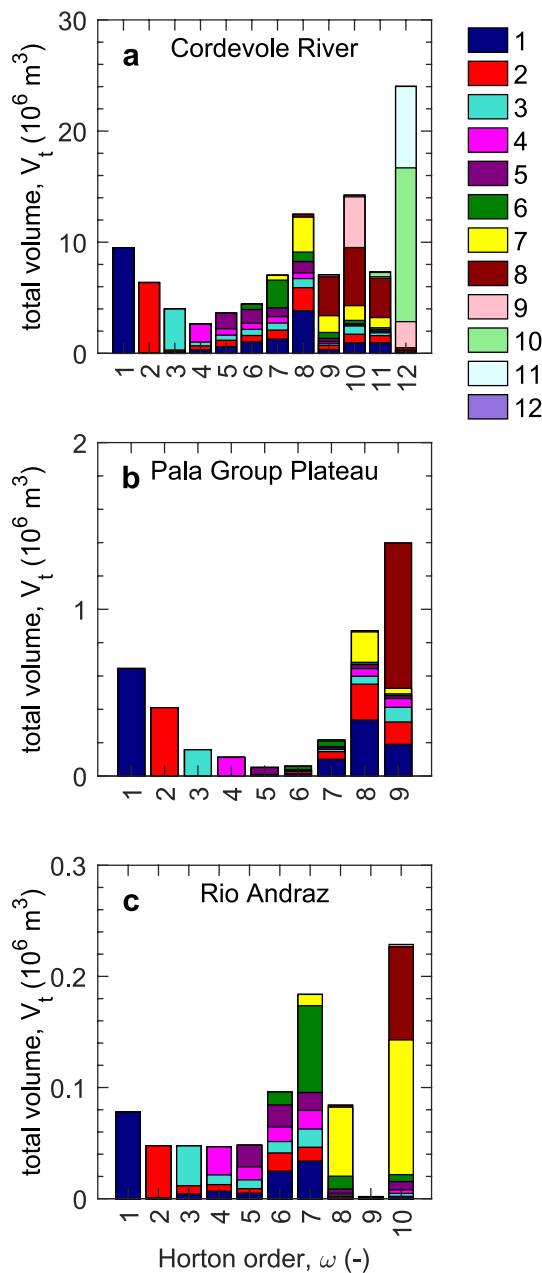


**Figure 11.** Total filling volumes  $V_t$  in subbasins drained by thalwegs having Horton order  $\omega$ , for the drainage basins highlighted in Figures 7–9 (a–c, respectively). Each bar reports the partial contributions of subbasins having orders less than or equal to  $\omega$  (colors indicated in the legend) that drain directly into the thalweg having order  $\omega$  and the total filling volume over all the subbasins having order  $\omega$  (bar length). Partial contributions of subbasins having order  $\omega$  are due to grid cells crossed by the thalweg having order  $\omega$ . The data plotted in (a–c) are reported in Tables S1–S3 in Supporting Information S1, respectively.

While thalwegs are identified by connecting cell centers along steepest slope directions, the identification of ridgelines is based only on relationships between neighboring ridge points lying along grid cell borders. In fact, no similar attributes as the steepest slope direction in thalweg junctions are available in ridgeline junctions to determine the joining and resulting ridgelines. As described in Section 2.4 and reported in Figure 5, the ridge network is identified by considering ridgeline starting points (close to thalweg junctions) in order of increasing elevation. From any given ridge point having only one neighboring ridge point that remains unconnected, the ridgeline extends toward this unconnected ridge point. When a ridge point having more than one neighboring ridge point that remains unconnected is found, a ridgeline junction is recognized and the extension of the ridgeline is stopped. The same junction is recognized by other ridgelines that are all stopped until the ridgeline junction has only one unconnected neighboring ridge point left. Then, the ridgeline continues from the ridgeline junction in the direction of the last neighboring ridge point unconnected. Ridgelines are identified from their lowermost ridge point to their uppermost ridge point by following a profile that generally displays fluctuations in elevation. As reported in Section 2.4, a two-step procedure that calls the first and second steps one after the other is needed to process ridge points having one neighboring ridge point in the first step and to handle depressions along the ridgeline in the second step, where ridge points that were skipped in the first step are reconsidered. The procedure ends when the highest peak of the considered geographical area is reached, that is, when the root of the ridge network having a tree structure is recognized. The consideration of ridgeline starting points in order of increasing elevation is essential to ensure the completeness of the ridge network. Ridgelines are characterized by their dispersal area. Results indicate that the hierarchization of ridgelines based on the dispersal area highlights the tree structure of the ridge networks and effectively describes the distribution of water and sediments exercised by ridges within a drainage basin and also between different drainage basins of a considered geographical area as shown in Figures 7–9.

The capabilities of the LANDMARK algorithm, as compared to existing terrain analysis methods, are made possible by three technical innovations. First, ridge points and specifically spilling saddles are identified along DEM cell borders by considering all grid cell border midpoints and vertices that are not crossed by slopelines (Figures 3–5). Second, spilling saddles are processed in order of increasing elevation to connect in a physically meaningful manner complex system of exorheic and endorheic basins by forming the thalweg network (Section 2.3). Third, ridgeline starting points (close to thalweg junctions) are processed in order of increasing elevation so that ridgelines are identified and ridgeline junctions are solved in a physically meaningful manner on the basis of relationships between neighboring ridge points by forming the complete ridge network (Section 2.4). With these innovations, the LANDMARK algorithm identifies the thalweg and ridge networks as would be made in the field by an observer interested in connecting exorheic and endorheic basins for the purpose of describing surface flow and storage processes and in connecting ridge points for the purpose of describing basins and subbasins contributing to the thalweg network (Sections 2.3 and 2.4). Observed topographic features are well reproduced by extracted networks

(Figures 7–9). In exorheic basins, the obtained thalweg network does not differ significantly from that extracted after DF (Figure 9 and Figure S1 in Supporting Information S1). However, the description of thalwegs within endorheic basins is made possible by the use of the LANDMARK algorithm in preference to DF (Figure 9). The LANDMARK algorithm is therefore essential to describe flow and storage effects within endorheic basins



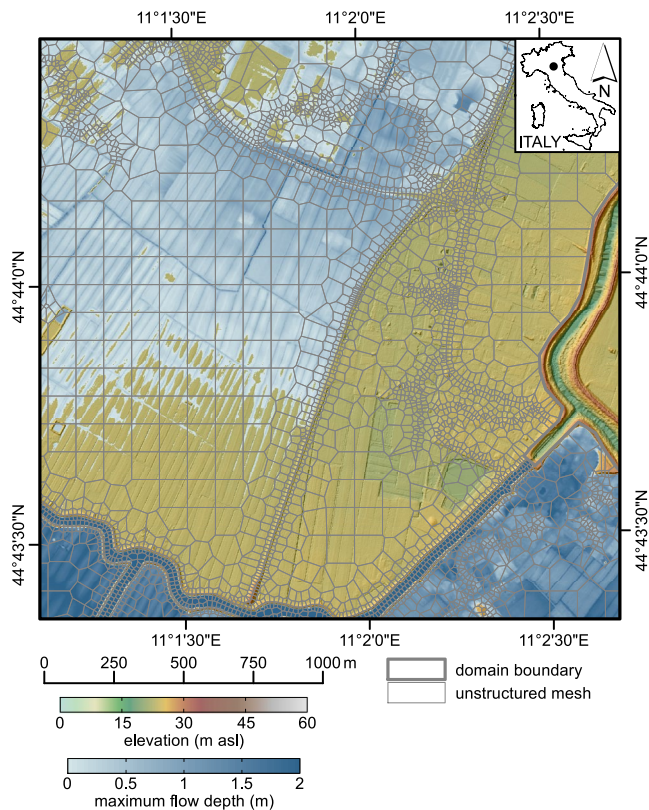


**Figure 12.** Terrain partitioning of lowland terrain located between the Secchia and Panaro Rivers (Po River valley, Italy) obtained by using an unstructured mesh that adapts to the ridge network extracted through the LANDMARK algorithm by setting  $S_c = 10^4 \text{ m}^2$  and related simulation of flooded areas during the event of 19 January 2014.

and across complex terrain composed of connected exorheic and endorheic basins. The characterization of thalweg and ridge networks in terms of drainage and dispersal areas leads to a realistic representation of the concentration (or drainage) and distribution (or spread) processes in drainage basins and across geographical areas (Figures 7–9). In a similar way as the drainage area indicates the concentration (or drainage) of flow exercised by thalwegs, the dispersal area indicates the distribution (or spread) of flow exercised by ridges.

The ability of the LANDMARK algorithm to handle complex systems of nested endorheic basins compared to standard terrain analysis methods can be appreciated by considering Figure 8. This figure shows that any endorheic basin is connected to an exorheic basin or to another endorheic basin by identifying all the saddles lying along the ridgeline delimiting the endorheic basin and by considering as a spilling saddle the one displaying the lowest elevation. For clarity of representation, only endorheic basins having an area greater than or equal to  $500 \text{ m}^2$  are considered. Depression filling algorithms essentially raise the land surface topography of depressions and endorheic basins to the level of the related spilling saddles (Figure S1 in Supporting Information S1). Although DF is commonly applied in drainage basin hydrology, with this alteration the terrain topography characterized by a complex system of nested exorheic and endorheic basins is lost and the description of surface flows and storages, as well as of surface–subsurface flow interactions suffers accordingly. Extracted thalweg and ridge networks can, for instance, inform the description of bifurcating flows such as those occurring in braided rivers or around large trees, buildings, and other macrotopographic structures, as well as hyporheic flows and seepage flows in levees in fluvial systems. In fact, extracted thalweg and ridge networks can be pruned and used to obtain unstructured meshes that retain the essential thalwegs (main flow paths) and ridges (barriers) observed in high-resolution topographic data. Bifurcating flows, hyporheic flows, and seepage flows can then be described separately using suitable hydraulic models as exemplified in Section 3.2. A new generation of models for the description of Earth surface processes can

be developed by preserving the essential information content (thalwegs and ridges) of high-resolution grid DEMs when terrain is partitioned and a computational mesh is generated (Figures 9 and 12). The preservation of observations is a basic requirement in any Earth and planetary science investigation. Terrain partitioning based on thalweg and ridge networks generalizes existing models for the description of Earth surface processes and allows scientists and engineers to evaluate in a scientifically sound manner when depressions can be filled for model simplicity and when they should rather be considered as a relevant factor in the investigated processes.

The Horton analysis of thalweg networks and related subbasins extracted from the 5-m grid DEM of the Cordevole River drainage basin after LANDMARK or DF algorithms are applied reveals the impact of preserving land surface depressions in a mountainous terrain (Figures 10 and 11). The logarithm of the number of thalwegs  $N$  is linearly related to the Horton order  $\omega$  as expected, with no significant differences between the LANDMARK and DF cases (Figure 10a). The value of the mean filling depth  $D_m$  reported in Figure 10b ranges from 8.6 mm, for  $\omega = 4$ , to 55.7 mm, for  $\omega = 11$ , and is therefore significant over the full range of the thalweg order  $\omega$ . In order to understand the patterns displayed by the variation of  $D_m$  with  $\omega$ , with high values for  $\omega = 1$  and for orders  $\omega$  close to the maximum order ( $\omega = 12$  in Figure 10b) and relatively low values for  $\omega = 4$ , the variation of mean drainage area  $A_m$ , mean filling volume  $V_m$ , total drainage area  $A_r$ , and total filling volume  $V_r$  are examined (Figure 10c–10f). The logarithm of  $A_m$  was found to vary linearly with  $\omega$  in both cases, with no significant differences between the LANDMARK and DF cases (Figure 10c). It is noted that  $A_m$  is equal to  $4,792 \text{ m}^2$  for  $\omega = 4$ , which corresponds to the critical drainage area for channel initiation observed in the same mountain region (Orlandini et al., 2011). The variation of the logarithm of  $V_m$  with  $\omega$  shown in Figure 10d displays a similar pattern, and this suggests that  $A_m$  exercises a greater influence on  $V_m$  (Figure 10d) than  $D_m$  (Figure 10b). The total drainage area  $A_r$  does not display a large variation with  $\omega$  for  $\omega \leq 8$  and varies irregularly with  $\omega$  for  $\omega > 8$  (Figure 10e). This explains why

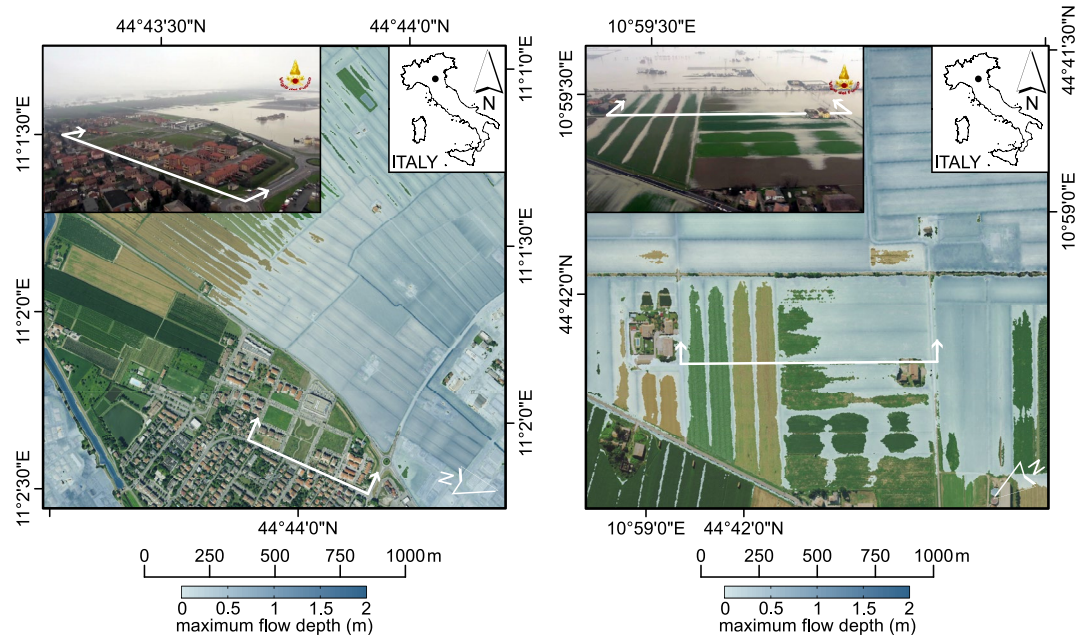


**Figure 13.** Comparison between simulated and observed flooded areas in the terrain located between the Secchia and Panaro Rivers (Po River valley, Italy) during the event of 19 January 2014. The terrain partitioning obtained using the automatically extracted ridge network reported in Figure 12 is essential to accurately describe man-made topographic structures such as road embankments and the related hydraulic effects on surface flow propagation.

the variations of the logarithm of  $V_i$  (Figure 10f) and of the logarithm of  $D_m$  (Figure 10b) with  $\omega$  display similar patterns. Fluctuations observed in  $D_m$ ,  $A_p$ , and  $V_i$  for  $\omega > 8$  (Figures 10b, 10e, and 10f, respectively) are an effect of the extension upslope of the Horton order of thalwegs, which significantly reduces the number of contributing drainage basins having order close to the maximum order (for instance, basins having order 11 in Figures 10 and 11). Similar results are obtained for the 1- and 5-m DEMs of the drainage basins highlighted in Figures 8 and 9, as reported in Figures S4 and S5 in Supporting Information S1, respectively.

The results reported in Figure 11 and Tables S1–S3 in Supporting Information S1 confirm that the minimum total filling volume  $V_i$  is observed in subbasins having order 4 or 5, with little contribution from subbasins having lower orders. In the cases considered in the present study, by examining the alterations of the observed topographic data, filling depths over subbasins having orders  $\omega$  less than 4 are generally found to be on the order of 1 cm or less. Exceptions are found when these subbasins are part of a larger endorheic basin. In these cases, the filling depth is determined by the increase in elevation needed to reach the elevation of the spilling saddle (Figure S1 in Supporting Information S1). It is therefore concluded that the relatively high contributions to  $V_i$  of subbasins having order  $\omega < 4$  is not due to their large number (Figure 10, Figures S5, S6, and Tables S4–S6 in Supporting Information S1) or to the combined effect of local depressions, but rather due to a relatively small number of these small subbasins falling within endorheic basins and raised to the elevations of the related spilling saddles. Endorheic basins are not generally found in subbasins having order  $\omega$  less than 4 or 5, and instead start to play a role in subbasins having higher orders. In fact, the increase in the total filling volume  $V_i$  for  $\omega > 4$  is not due to the increase in the total drainage area  $A_i$ , as this quantity is found to be almost constant around values of  $\omega$  of 4 or 5, but rather due to the impact of endorheic basins. This is confirmed by the analysis of small contributions to  $V_i$  of the subbasin having order 9 in Figure 11c and Figure S5f in Supporting Information S1. In fact, the subbasin having order 9 in the drainage basin highlighted in Figure 9 displays a small total filling volume in accordance with the absence of endorheic basins observed in this subbasin. The preservation of depressions observed in topographic data is found to have little effect on the Horton planimetric properties of thalweg networks (Figure 10, Figures S4, and S5 in Supporting Information S1), but is found to have a significant impact on the description of relief as suggested by filling depths and volumes observed across drainage basins (Figures 10 and 11, Figures S4–S6, and Tables S1–S6 in Supporting Information S1). The major impact of DF in terms of volumes is due to endorheic drainage basins rather than small (natural or artificial) depressions at the grid cell scale that are

distributed across exorheic basins. Future research, however, is needed to generalize existing models for the description of Earth surface processes and to determine the circumstances under which depressions may or may not be filled for model simplicity.

Thalweg and ridge networks represented at the desired level of detail can be used as bases for terrain partitioning. In Figure 6, the thalweg and ridge networks are extracted at the maximum level of detail offered by the grid DEM and the terrain is partitioned accordingly. The LANDMARK algorithm, however, is designed to capture the essential topographic features represented in high-resolution grid DEMs while also supporting the generation of unstructured computational meshes that are compatible with the efficiency requirements of models for the description of Earth surface processes. Under this perspective, the full thalweg and ridge networks obtained from the best available high-resolution grid DEM can be pruned on the basis of the displayed values of drainage and dispersal areas. Pruned thalweg networks are obtained by considering only those thalwegs displaying a drainage area greater than or equal to a critical drainage area for thalweg representation  $A_c$  (Figures 7–9 and Figure S2 in Supporting Information S1). Pruned ridge networks can be obtained in three ways. First, only ridgelines beginning at the thalweg junctions of a pruned thalweg network are considered (Figures 7 and 9, Figure S3 in Supporting Information S1). In Figures 7 and 9, for instance, thalweg and ridge networks are obtained by setting  $A_c = 10^6 \text{ m}^2$ . Second, only ridgelines beginning at spilling saddles and delimiting endorheic basins are considered (Figure 8). Third, pruned ridge networks are obtained by considering only those ridges displaying a dispersal area greater than or equal to a critical dispersal area for ridge representation  $S_c$  (Figure 12). In all cases, thalweg and ridge networks can be used as breaklines to support the generation of a physically meaningful terrain partitioning (Figures 6, 9, and 12). The related mesh preserves the structure of the thalweg and ridge networks by using small elements only when they are needed to describe the terrain complexity and by using relatively large elements when the topographic detail is not strictly needed (Figures 9 and 12). Clearly, the selection of the level of detail in the description of thalweg and ridge networks, as well as in the generation of the related terrain partitioning, is a matter of choice in balancing model accuracy and computational efficiency.

The benefits of using unstructured computational meshes based on extracted thalweg and ridge networks in HEC-RAS 2D flood inundation models are shown by considering the lowland terrain located between the Secchia and Panaro Rivers and the flood event of 19 January 2014 (Figure 12). The automated procedure described in Section 2 leads to satisfactory results. The pruned ridge network obtained by setting  $S_c = 10^4 \text{ m}^2$  yields an accurate delineation of relevant ridges representing natural and man-made embankments (Figure 12). The unstructured mesh adapting to the extracted ridge network is composed of elements having variable size, ranging from about 10 m, where small elements are needed to accurately describe the extracted ridge network, to 100 m, where large grid cells are adequate to describe regular terrain. The small elements of the unstructured mesh (Figure 12) have about the same size as those of a 10-m regular grid (Figure S8 in Supporting Information S1), but only the former have facets that accurately adapt to the extracted ridges. The description of surface flow propagation and related inundation maps is found to be equally accurate when the automated LANDMARK algorithm and the manual delineations of breaklines are used (Figures 12 and 13, Figure S7 in Supporting Information S1). Although in simple cases the LANDMARK algorithm is not strictly needed to incorporate ridges observed in high-resolution topographic data into HEC-RAS 2D as breaklines, use of the algorithm ensures in all cases that this process is performed accurately and automatically, including in complex cases where manual delineation of ridges is not possible. Unstructured meshes obtained from breaklines delineating natural and man-made embankments (Figures 12 and 13, Figure S7 in Supporting Information S1) yield significantly more accurate results than a regular grid having a resolution of 10 m (Figure 13 and Figure S8 in Supporting Information S1). When the 10-m regular grid is used, HEC-RAS 2D is unable to accurately assimilate the embankments observed in the 1-m DEM because grid cell facets are generally not aligned with these topographic structures. Embankments are not accurately assimilated by HEC-RAS 2D as barriers to flow and the flow simulation suffers accordingly (Figure 13 and Figure S8 in Supporting Information S1). Even comparing cases where simulations based on LANDMARK are significantly more accurate than those based on a regular grid, computational efficiency is found to be considerably improved (wall-clock times 37 times smaller in the examined case) when an unstructured mesh (wall-clock time of 10.52 s/km<sup>2</sup>, Section 3.2) is used in preference to a regular grid (wall-clock time of 390.87 s/km<sup>2</sup>, Section 3.2). Surface flow simulations based on the LANDMARK algorithm are considerably more accurate and faster than those based on a reasonable regular grid. This is clearly due to the LANDMARK algorithm's ability to better describe the land surface topography by using a smaller number of computational elements (379 elements/km<sup>2</sup>) than regular grids (10,061 cells/km<sup>2</sup>). The use of unstructured meshes obtained

from the LANDMARK algorithm therefore provides a new pathway for scientists and engineers to rigorously incorporate detailed topographic data into their descriptions of surface flow propagation.

## 5. Conclusions

The present study shows that physically meaningful thalweg and ridge networks can be extracted automatically from any high-resolution grid DEM without the need to fill depressions in the observed topographic data (Figures 7–9 and Figures S1–S3 in Supporting Information S1). The developed algorithm is named LANDMARK because thalweg and ridge networks are thought to be essential topographic features (landmarks) for terrain partitioning (Figures 6, 9, and 12). The potential of the LANDMARK algorithm is shown over mountainous terrain in near-natural conditions located in the Italian Alps (Figures 7–11 and Figures S1–S6 in Supporting Information S1), and over a man-altered flood plain region located along the Po River valley (Figures 12 and 13, Figures S7 and S8 in Supporting Information S1). Observed topographic features are well reproduced by extracted networks (Figures 7–9 and 12). In the mountainous terrain, the preservation of depressions observed in topographic data is found to have little effect on the Horton planimetric properties of thalweg networks (Figure 10, Figures S4 and S5 in Supporting Information S1), but is found to have a significant impact on the description of relief as suggested by filling depths and volumes observed across drainage basins of any order, especially where endorheic basins exist (Figures 10 and 11, Figures S4–S6, and Tables S1–S6 in Supporting Information S1). In the flood plain region, the use of unstructured meshes based on the extracted ridge network leads to significantly more accurate flood simulations than those obtained by using regular grids due to a more detailed representation of critical topographic structures, while also ensuring a considerable gain in computational efficiency (at least 37 times faster simulations) due to the use of large mesh elements when topographic detail is not needed (Figures 12 and 13, Figures S7 and S8 in Supporting Information S1). It is therefore concluded that the developed terrain analysis methods provide a new pathway for scientists and engineers to rigorously incorporate detailed topographic data into their descriptions of Earth surface processes.

## Appendix A: Pseudocode for the Determination of Ridge Points

Procedure RIDGE POINTS

**Require:** High-resolution grid digital elevation model (DEM)

**Ensure:** Slopeline network, Ridge points, Average rejunction lengths, Exorheic and endorheic basins, Troughs, Outlets

CC = DEM cell center

CBP = DEM cell border point, either edge midpoint or vertex

SLOPELINE = steepest descent path from a cell to a trough or outlet

OCC = outlet cell center

TCC = troughcell center

RP = ridge point lying on a DEM cell border

ZRP = ridge point elevation

HL =  $10^{12}$  m, huge length

ARL = average rejunction length of the two slopelines extending on the opposite slopes of the ridge from the ridge point's closest cell centers, computed if these slopelines join or conventionally set equal to HL if these slopelines do not join within the considered domain

**for all** CC processed in order of decreasing elevation **do**  
 steepest slope direction determined using the D8-LTD method  
**if** the cell having center CC drains to a neighboring cell **then**  
 SLOPELINE ← CC

**else**

{no draining cells exist}

**if** the cell having center CC is on the edges of DEM **then**  
 {CC is necessarily the center of an outlet cell}

OCC = CC

the slopeline network contributing to OCC is determined

```

        {an exorheic basin is identified}
    else
        {CC is a trough}
        TCC = CC
        the slopeline network contributing to TCC is determined
        {an endorheic basin is identified}
    end if
end if
end for
for all CBP that does not lay on a slopeline do
    RP = CBP
    {RP is CBP not belonging to slopelines}
    ZRP = maximum elevation of neighboring CC to RP
    if RP is the midpoint of the cell edge then
        {two neighboring CC to RP are considered}
        the ARL between the neighboring CC is computed
    else
        {RP is a cell vertex}
        {up to four neighboring CC to RP are considered}
        the ARL between each couple of opposite CC with respect to RP is
        computed and the maximum ARL is recorded
    end if
end for
return

```

## Appendix B: Pseudocode for the Determination of the Thalweg Network

Procedure THALWEG NETWORK

**Require:** Slopelines, Ridge points, Average rejunction lengths, Exorheic and endorheic basins

**Ensure:** Saddles, Spilling saddles, Spilling saddle paths, Thalweg network

RP = ridge point

SLOPELINE = steepest descent path from a cell to a trough or outlet

SLOPELINE\_EXO = slopeline ending in an exorheic basin outlet

SLOPELINE\_ENDO = slopeline ending in an endorheic basin trough

HL =  $10^{12}$  m, huge length

ARL = average rejunction length of the two slopelines extending on the opposite slopes of the ridge from the ridge point's closest cell centers, computed if these slopelines join or conventionally set equal to HL if these slopelines do not join within the considered domain

S = saddle

ZS = saddle elevation

SS = spilling saddle

NESTED = priority queue for nested endorheic basins

**for all** RP having ARL = HL **do**

{RP dividing exorheic basins having different outlets or a endorheic basin from an adjacent (exorheic or endorheic) basin}

**for all** RP dividing two given adjacent basins **do**

S = RP having the minimum elevation

**end for**

**end for**

**for all** S processed in order of increasing elevation **do**

**if** S divides an endorheic basin from an exorheic basin **then**

```

{S is a spilling saddle}
SS = S
ZMAX = ZS
SLOPELINE_EXO = slope of an exorheic basin beginning at the closest cell center to S and ending at the exorheic basin outlet
SLOPELINE_ENDO = slope of an endorheic basin beginning at the closest cell center to S and ending at the endorheic basin trough
SPILLING_PATH = path connecting an endorheic basin trough to an exorheic basin outlet along a SLOPELINE_ENDO (traveled in a upslope direction) and a SLOPELINE_EXO (traveled in a downslope direction)
The connected endorheic basin is conceptually classified as a new portion of the draining exorheic basin
for all S of the new portion of the draining exorheic basin do
  if ZS < ZMAX then
    NESTED ← S in order of increasing elevation, with elevation equality solved by a first-in-first-out subqueue
    while NESTED is not empty do
      for all S belonging to NESTED do
        S is removed from NESTED
        if S divides an endorheic basin from an exorheic basin then
          {S is a spilling saddle}
          SS = S
          SLOPELINE_EXO = slope of an exorheic basin beginning at the closest cell center to S and ending at the exorheic basin outlet
          SLOPELINE_ENDO = slope of an endorheic basin beginning at the closest cell center to S and ending at the endorheic basin trough
          SPILLING_PATH = path connecting an endorheic basin trough to an exorheic basin outlet along a SLOPELINE_ENDO (traveled in a upslope direction) and a SLOPELINE_EXO (traveled in a downslope direction)
          The connected endorheic basin is conceptually classified as a new portion of the draining exorheic basin
          for all S of the new portion of the draining exorheic basin do
            if ZS < ZMAX then
              NESTED ← S in order of increasing elevation, with elevation equality solved by a first-in-first-out subqueue
            end if
          end for
        end if
      end for
    end while
  end if
end for

```

Slopes and spilling saddle paths form the thalweg network.

### Appendix C: Pseudocode for the Determination of the Ridge Network

Procedure RIDGE NETWORK

**Require:** Ridge points, Spilling saddles

```

Ensure: Ridgelines, Ridge network
RP = ridge point
SS = spilling saddle
URP = number of unconnected neighboring ridge points
ZRP = ridge point elevation
NEIGHBOR_RP = unconnected neighboring ridge point to a ridge point having
URP = 1
END_RP = ridge point ending a given ridgeline
RIDGELINE = ridgeline
for all SS do
  The RP corresponding to SS is conceptually split into two ancillary RP
end for
for all RP do
  URP = number of neighboring ridge points unconnected to the ridgeline
end for
for all RP processed in order of increasing elevation do
if URP = 1 then
  {RP has only one unconnected neighboring RP}
  FLAG = 1
  ZMAX = ZRP
  END_RP = RP
  if RP does not belong to a ridgeline then
    {A new ridgeline is initiated}
    RIDGELINE ← END_RP
  else
    {RP is already connected to a ridgeline}
    RIDGELINE = ridgeline containing END_RP
  end if
  while FLAG = 1 do
    NEIGHBOR_RP = the unconnected neighboring RP
    RIDGELINE ← NEIGHBOR_RP
    END_RP = NEIGHBOR_RP
    if URP(END_RP) = 1 and ZRP(END_RP) ≤ ZMAX then
      {END_RP has only one unconnected neighboring RP and END_RP has eleva-
      tion less than or equal to ZMAX, indicating that the ridgeline does
      not vary monotonically in elevation}
      FLAG = 1
    else
      FLAG = 0
    end if
  end while
end if
end for
Ridgelines form the ridge network.

```

### Conflict of Interest

The authors declare no conflicts of interest relevant to this study.

### Data Availability Statement

Data and FORTRAN codes used to generate the results reported in this manuscript are available on Zenodo at <https://zenodo.org/record/7037277> (Moretti & Orlandini, 2022).

### Acknowledgments

The research reported in the present paper was supported by Fondazione Cassa di Risparmio di Modena through the Grant 2018-0093, by the University of Modena and Reggio Emilia through the Grant FAR 2020 Mission Oriented, and by the European Union NextGenerationEU/NRRP, Mission 4 Component 2 Investment 1.5, Call 3277 (12/30/2021), Award 0001052 (06/23/2022), under the project ECS00000033 “Ecosystem for Sustainable Transition in Emilia-Romagna.” Spoke 6 “Ecological Transition Based on HPC and Data Technology.” High-resolution topographic data were provided by Ministero dell’Ambiente, della Tutela del Territorio e del Mare (Rome, Italy), Regione del Veneto (Venice, Italy), Provincia Autonoma di Trento (Trento, Italy), and Provincia Autonoma di Bolzano (Bolzano, Italy), for the Cordevole River drainage basin, and by Ministero dell’Ambiente, della Tutela del Territorio e del Mare (Rome, Italy), Agenzia Interregionale per il Fiume Po (Parma, Italy), and Regione Emilia-Romagna (Bologna, Italy), for the Po Valley flood plain. The observations of the flood event that occurred along the Po Valley flood plain on 19 January 2014 were provided by the Civil Protection of the Regione Emilia-Romagna (Italy) and by the National Fire and Rescue Service (Modena, Italy). The authors thank the Editor Mikael Attal, the anonymous Associate Editor, and three anonymous reviewers for comments that led to improvements in the manuscript. Open Access Funding provided by Università degli Studi di Modena e Reggio Emilia within the CRUI-CARE Agreement.

### References

- Barnes, R., Callaghan, K. L., & Wickert, A. D. (2020). Computing water flow through complex landscapes—Part 2: Finding hierarchies in depressions and morphological segmentations. *Earth Surface Dynamics*, 8(2), 431–445. <https://doi.org/10.5194/esurf-8-431-2020>
- Barnes, R., Callaghan, K. L., & Wickert, A. D. (2021). Computing water flow through complex landscapes—Part 3: Fill–spill–merge: Flow routing in depression hierarchies. *Earth Surface Dynamics*, 9(1), 105–121. <https://doi.org/10.5194/esurf-9-105-2021>
- Barnes, R., Lehman, C., & Mulla, D. (2014). Priority-flood: An optimal depression-filling and watershed-labeling algorithm for digital elevation models. *Computers & Geosciences*, 62(1), 117–127. <https://doi.org/10.1016/j.cageo.2013.04.024>
- Black, B. A., Perron, J. T., Hemingway, D., Bailey, E., Nimmo, F., & Zebker, H. (2017). Global drainage patterns and the origins of topographic relief on Earth, Mars, and Titan. *Science*, 356(6339), 727–731. <https://doi.org/10.1126/science.aag0171>
- Burr, D. (2017). Defining the topography of a planetary body. *Science*, 356(6339), 708. <https://doi.org/10.1126/science.aan2719>
- Callaghan, K. L., & Wickert, A. D. (2019). Computing water flow through complex landscapes—Part 1: Incorporating depressions in flow routing using flowfill. *Earth Surface Dynamics*, 7(3), 737–753. <https://doi.org/10.5194/esurf-7-737-2019>
- Cayley, A. (1859). On contour and slope lines. *The London, Edinburgh, and Dublin Philosophical Magazine and Journal of Science*, 18(120), 264–268. <https://doi.org/10.1080/14786445908642760>
- Chang, Y.-C., Song, G.-S., & Hsu, S.-K. (1998). Automatic extraction of ridge and valley axes using the profile recognition and polygon-breaking algorithm. *Computers & Geosciences*, 24(1), 83–93. [https://doi.org/10.1016/S0098-3004\(97\)00078-2](https://doi.org/10.1016/S0098-3004(97)00078-2)
- Chen, Y., Wilson, J. P., Zhu, Q., & Zhou, Q. (2012). Comparison of drainage-constrained methods for DEM generalization. *Computers & Geosciences*, 48(Supplement C), 41–49. <https://doi.org/10.1016/j.cageo.2012.05.002>
- Costa-Cabral, M., & Burges, S. J. (1994). Digital elevation model networks (DEMONT): A model of flow over hillslopes for computation of contributing and dispersal areas. *Water Resources Research*, 30(6), 1681–1692. <https://doi.org/10.1029/93wr03512>
- David, S. R., Murphy, B. P., Czuba, J. A., Ahammad, M., & Belmont, P. (2023). USUAL watershed tools: A new geospatial toolkit for hydro-geomorphic delineation. *Environmental Modelling & Software*, 159, 105576. <https://doi.org/10.1016/j.envsoft.2022.105576>
- Dawes, W. R., & Short, D. (1994). The significance of topology for modeling the surface hydrology of fluvial landscapes. *Water Resources Research*, 30(4), 1045–1055. <https://doi.org/10.1029/93wr02479>
- Di Martire, D., Paci, M., Confuorto, P., Costabile, S., Guastaferrò, F., Verta, A., & Calcaterra, D. (2017). A nation-wide system for landslide mapping and risk management in Italy: The second not-ordinary plan of environmental remote sensing. *International Journal of Applied Earth Observation and Geoinformation*, 63(12), 143–157. <https://doi.org/10.1016/j.jag.2017.07.018>
- Frolking, S., Palace, M., Clark, D., Chambers, J., Shugart, H., & Hurr, G. (2009). Forest disturbance and recovery: A general review in the context of spaceborne remote sensing of impacts on aboveground biomass and canopy structure. *Journal of Geophysical Research*, 114(G2), 27. <https://doi.org/10.1029/2008JG000911>
- Grimaldi, S., Nardi, F., Di Benedetto, F., Istanbuluoglu, E., & Bras, R. L. (2007). A physically-based method for removing pits in digital elevation models. *Advances in Water Resources*, 30(10), 2151–2158. <https://doi.org/10.1016/j.advwatres.2006.11.016>
- Head, J. W., Mustard, J. F., Kreslavsky, M. A., Milliken, R. E., & Marchant, D. R. (2003). Recent ice ages on Mars. *Nature*, 426(6968), 797–802. <https://doi.org/10.1038/nature02114>
- Horton, R. E. (1945). Erosional development of streams and their drainage basins: Hydrophysical approach to quantitative morphology. *Geological Society of America Bulletin*, 56(3), 275–370. [https://doi.org/10.1130/0016-7606\(1945\)56\[275:edosatl\]2.0.co;2](https://doi.org/10.1130/0016-7606(1945)56[275:edosatl]2.0.co;2)
- Hutchinson, M. F. (1989). A new procedure for gridding elevation and stream line data with automatic removal of spurious pits. *Journal of Hydrology*, 106(1–2), 221–232. [https://doi.org/10.1016/0022-1694\(89\)90073-5](https://doi.org/10.1016/0022-1694(89)90073-5)
- Hydrologic Engineering Center. (2016). *HEC-RAS: River analysis system (hydraulic reference manual)*. US Army Corps of Engineers Hydrologic Engineering Center.
- Hydrologic Engineering Center. (2020). *Modeler application guidance for steady vs unsteady, and 1D vs 2D vs 3D hydraulic modeling (training document)*. US Army Corps of Engineers Hydrologic Engineering Center.
- Hydrologic Engineering Center. (2022). *Development of the 2D computational mesh (training document)*. US Army Corps of Engineers Hydrologic Engineering Center.
- Ivanov, V. Y., Vivoni, E. R., Bras, R. L., & Entekhabi, D. (2004). Catchment hydrologic response with a fully distributed triangulated irregular network model. *Water Resources Research*, 40(11), W11102. <https://doi.org/10.1029/2004WR003218>
- Leopold, L. B., Wolman, M. G., & Miller, J. P. (1964). *Fluvial processes in geomorphology*. W. H. Freeman.
- Lindsay, J. B., & Creed, I. F. (2005). Removal of artifact depressions from digital elevation models: Towards a minimum impact approach. *Hydrological Processes*, 19(16), 3113–3126. <https://doi.org/10.1002/hyp.5835>
- Lindsay, J. B., & Seibert, J. (2012). Measuring the significance of a divide to local drainage patterns. *International Journal of Geographical Information Science*, 27(7), 1453–1468. <https://doi.org/10.1080/13658816.2012.705289>
- Martz, L. W., & de Jong, E. (1987). Using Cesium-137 to assess the variability of net soil erosion and its association with topography in a Canadian Prairie landscape. *Catena*, 14(5), 439–451. [https://doi.org/10.1016/0341-8162\(87\)90014-2](https://doi.org/10.1016/0341-8162(87)90014-2)
- Martz, L. W., & Garbrecht, J. (1992). Numerical definition of drainage network and subcatchment areas from digital elevation models. *Computers & Geosciences*, 18(6), 747–761. [https://doi.org/10.1016/0098-3004\(92\)90007-e](https://doi.org/10.1016/0098-3004(92)90007-e)
- Martz, L. W., & Garbrecht, J. (1999). An outlet breaching algorithm for the treatment of closed depressions in a raster DEM. *Computers & Geosciences*, 25(7), 835–844. [https://doi.org/10.1016/S0098-3004\(99\)00018-7](https://doi.org/10.1016/S0098-3004(99)00018-7)
- Maunder, C. J. (1999). An automated method for constructing contour-based digital elevation models. *Water Resources Research*, 35(12), 3931–3940. <https://doi.org/10.1029/1999wr900166>
- Maxwell, J. C. (1870). On hills and dales. *The London, Edinburgh, and Dublin Philosophical Magazine and Journal of Science*, 40(269), 421–425. <https://doi.org/10.1080/14786447008640422>
- Moore, I. D., & Grayson, R. B. (1991). Terrain-based catchment partitioning and runoff prediction using vector elevation data. *Water Resources Research*, 27(6), 1177–1191. <https://doi.org/10.1029/91wr00090>
- Moore, I. D., O’Loughlin, E. M., & Burch, G. J. (1988). A contour-based topographic model for hydrological and ecological applications. *Earth Surface Processes and Landforms*, 13(4), 305–320. <https://doi.org/10.1002/esp.3290130404>
- Moretti, G., & Orlandini, S. (2008). Automatic delineation of drainage basins from contour elevation data using skeleton construction techniques. *Water Resources Research*, 44(5), W05403. <https://doi.org/10.1029/2007WR006309>
- Moretti, G., & Orlandini, S. (2018). Hydrography-driven coarsening of grid digital elevation models. *Water Resources Research*, 54(5), 3654–3672. <https://doi.org/10.1029/2017WR021206>
- Moretti, G., & Orlandini, S. (2022). Identification of thalweg and ridge networks as landmarks for terrain partitioning. *Zenodo*. <https://doi.org/10.5281/zenodo.7037277>



- O'Callaghan, J., & Mark, D. M. (1984). The extraction of drainage networks from digital elevation data. *Computer Vision, Graphics, and Image Processing*, 28(3), 323–344. [https://doi.org/10.1016/s0734-189x\(84\)80047-x](https://doi.org/10.1016/s0734-189x(84)80047-x)
- O'Donnell, G., Nijssen, G. B., & Lettenmaier, D. P. (1999). A simple algorithm for generating streamflow networks for grid-based, macroscale hydrological models. *Hydrological Processes*, 13(8), 1269–1275. [https://doi.org/10.1002/\(sici\)1099-1085\(19990615\)13:8<1269::aid-hyp806>3.0.co;2-r](https://doi.org/10.1002/(sici)1099-1085(19990615)13:8<1269::aid-hyp806>3.0.co;2-r)
- O'Loughlin, E. M. (1986). Prediction of surface saturation zones in natural catchments by topographic analysis. *Water Resources Research*, 22(5), 794–804. <https://doi.org/10.1029/wr022i005p00794>
- Onstad, C. A., & Brakensiek, D. L. (1968). Watershed simulation by stream path analogy. *Water Resources Research*, 4(5), 965–971. <https://doi.org/10.1029/wr004i005p00965>
- Orlandini, S., Moretti, G., & Albertson, J. D. (2015). Evidence of an emerging levee failure mechanism causing disastrous floods in Italy. *Water Resources Research*, 51(10), 7995–8011. <https://doi.org/10.1002/2015WR017426>
- Orlandini, S., Moretti, G., Franchini, M., Aldighieri, B., & Testa, B. (2003). Path-based methods for the determination of nondispersive drainage directions in grid-based digital elevation models. *Water Resources Research*, 39(6), 1144. <https://doi.org/10.1029/2002WR001639>
- Orlandini, S., Moretti, G., & Gavioli, A. (2014). Analytical basis for determining slope lines in grid digital elevation models. *Water Resources Research*, 50(1), 526–539. <https://doi.org/10.1002/2013WR014606>
- Orlandini, S., Tarolli, P., Moretti, G., & Dalla Fontana, G. (2011). On the prediction of channel heads in a complex alpine terrain using gridded elevation data. *Water Resources Research*, 47(2), W02538. <https://doi.org/10.1029/2010WR009648>
- Passalacqua, P., Belmont, P., Staley, D. M., Simley, J. D., Arrowsmith, J. R., Bode, C. A., et al. (2015). Analyzing high resolution topography for advancing the understanding of mass and energy transfer through landscapes: A review. *Earth-Science Reviews*, 148, 174–193. <https://doi.org/10.1016/j.earscirev.2015.05.012>
- Perron, J. T., Kirchner, J. W., & Dietrich, W. E. (2009). Formation of evenly spaced ridges and valleys. *Nature*, 460(7254), 502–505. <https://doi.org/10.1038/nature08174>
- Perron, J. T., Mitrovica, J. X., Manga, M., Matsuyama, I., & Richards, M. A. (2007). Evidence for an ancient Martian ocean in the topography of deformed shorelines. *Nature*, 447(7146), 840–843. <https://doi.org/10.1038/nature05873>
- Rak, R., Kwapien, J., Oświęcimka, P., Zięba, P., & Drożdż, S. (2019). Universal features of mountain ridge networks on Earth. *Journal of Complex Networks*, 8(1), cnz017. <https://doi.org/10.1093/comnet/cnz017>
- Rana, S. (2006). Use of plan curvature variations for the identification of ridges and channels on DEM. In *Progress in spatial data handling 12th international symposium on spatial data handling* (pp. 789–804). Springer.
- Reed, S. M. (2003). Deriving flow directions for coarse-resolution (1–4 km) gridded hydrologic modeling. *Water Resources Research*, 39(9), 558. <https://doi.org/10.1029/2003WR001989>
- Robinson, S., Bohon, W., Kleber, E., Arrowsmith, J., & Crosby, C. (2017). Applications of high-resolution topography in Earth science education. *Geosphere*, 13(6), 1887–1900. <https://doi.org/10.1130/GES01236.1>
- Shugart, H., Saatchi, S., & Hall, F. (2010). Importance of structure and its measurement in quantifying function of forest ecosystems. *Journal of Geophysical Research*, 115(G2), 16. <https://doi.org/10.1029/2009JG000993>
- Smith, D. E., Zuber, M. T., Solomon, S. C., Phillips, R. J., Head, J. W., Garvin, J. B., et al. (1999). The global topography of Mars and implications for surface evolution. *Science*, 284(5419), 1495–1503. <https://doi.org/10.1126/science.284.5419.1495>
- Tarolli, P. (2014). High-resolution topography for understanding Earth surface processes: Opportunities and challenges. *Geomorphology*, 216(7), 295–312. <https://doi.org/10.1016/j.geomorph.2014.03.008>
- Vivoni, E. R., Ivanov, V. Y., Bras, R. L., & Entekhabi, D. (2004). Generation of triangulated irregular networks based on hydrological similarity. *Journal of Hydrologic Engineering*, 9(4), 288–303. [https://doi.org/10.1061/\(asce\)1084-0699\(2004\)9:4\(288\)](https://doi.org/10.1061/(asce)1084-0699(2004)9:4(288))
- Werner, C. (1972). Channel and ridge networks in rainage basins. *Proceedings of the Association of American Geographers*, 4, 109–114.
- Werner, C. (1988). Formal analysis of ridge and channel patterns in maturely eroded terrain. *Annals of the Association of American Geographers*, 78(2), 253–270. <https://doi.org/10.1111/j.1467-8306.1988.tb00206.x>
- Willett, S. D., McCoy, S. W., Perron, J. T., Goren, L., & Chen, C.-Y. (2014). Dynamic reorganization of river basins. *Science*, 343(6175), 1248765. <https://doi.org/10.1126/science.1248765>
- Zevenbergen, L. W., & Thorne, C. R. (1987). Quantitative analysis of land surface topography. *Earth Surface Processes and Landforms*, 12(1), 47–56. <https://doi.org/10.1002/esp.3290120107>
- Zhang, Y., & Jia, Y. (2020). Watershed merging: A simple and effective algorithm for channel network identification and extraction. *Water Resources Research*, 56(10), e2019WR026943. <https://doi.org/10.1029/2019WR026943>
- Zhou, Q., & Chen, Y. (2011). Generalization of DEM for terrain analysis using a compound method. *ISPRS Journal of Photogrammetry and Remote Sensing*, 66(1), 38–45. <https://doi.org/10.1016/j.isprsjprs.2010.08.005>